國立交通大學

電子工程學系 電子研究所碩士班

碩士論文

對於電化學沉積的氧化亞銅/二氧化鈦塊材異質接面特性的研究

Characterization of Electrochemically Deposited Cu_2O/TiO_2 Bulk Hetero-Junction

研 究 生：許文朋

指導教授：簡昭欣 教授

中華民國 九十八 年 九 月

對於電化學沉積的氧化亞銅/二氧化鈦塊材異質接面特性的研究

Characterization of Electrochemically Deposited Cu_2O/TiO_2 Bulk Hetero-Junction

研究生：許文朋 Student：Wen-Peng Hsu

指導教授：簡昭欣 Advisor：Chao-Hsin Chien

國立交通大學

電子工程學系 電子研究所碩士班

碩士論文

A Thesis
Submitted to Department of Electronics Engineering & Institute of Electronics
College of Electrical Engineering and Computer Engineering
National Chiao Tung University
In Partial Fulfillment of the Requirements
For the Degree of
Master
In
Electronics Engineering
September 2009
Hsinchu, Taiwan

中華民國九十八年九月

對於電化學沉積的氧化亞銅/二氧化鈦塊材異質接面特性的研究

研究生：許文朋　　　　　　　　　指導教授：簡昭欣 教授

國立交通大學

電子工程學系　電子研究所碩士班

摘要

由於染料敏化太陽能電池的低製造成本以及較短的能源償還期特性，對於能源的應用來講它是一種很吸引人的選擇。但是封裝膜的劣化所造成的電解液漏液的問題是很難避免的。為了要進一步改善染料敏化電池長期使用的穩定性，固態材料或許可以用來替代液態的電解液層。在這篇論文中，氧化亞銅被用來當作電洞傳輸層而且很成功的形成氧化亞銅/二氧化鈦塊材異質接面。

首先，用電化學沉積法將氧化亞銅沉積在奈米多孔狀的二氧化鈦膜中。由於沉積條件是和我們所要沉積上去的物質的表面特性息息相關，所以不容易找到最佳的沉積條件。因此，材料分析扮演了一個很重要的角色。藉由X-光光電子儀以及X-射線繞射光譜儀，我們可以從各種沉積條件中去找出最佳的條件。此外，藉由掃描電子顯微鏡我們可以觀察到沉積的速率。我們相信所有的材料分析技術可以幫助我們成功地去行形成氧化亞銅/二氧化鈦塊材異質接面。

接著，藉由光電量測以及電阻抗儀，我們研究了這個塊材異質接面的基本特性。由我們得到的結果中，復合機制被認為是限制這個接面表現的主要原因。在運用到染料敏化太陽能電池之前，對於復合中心數量的抑制是很重要的。因此，我們測試了很多條件以進一步的減少復合電流。藉由電阻抗儀的量測，我們從復合機制對於頻率的響應去研究復合機制的變化，並試著找到最好的方法來改善接面的表現。

對於氧化亞銅/二氧化鈦塊材異質接面有了初步的了解後，我們做了一些進階的量測來研究這個接面的其他特性。首先，藉由提高溫度來檢驗這個接面對於溫度的相依性。接著，用不同的衰減片來調整光的強度，並研究這個接面在不同照光強度下的影響。最後，我們分析接面對於電壓的響應，並由電阻抗儀的結果來得到我們所要的莫特-蕭特基圖。藉由莫特-蕭特基的結果，我們可以得到平帶電壓並且構建出完整的能帶模型。

在本論文中，我們藉由電化學沉積法以及適當的沉積條件，成功地形成了氧化亞銅/二氧化鈦塊材異質接面。並且由直流的電流-電壓量測和交流的電阻抗儀量測來觀察這個接面的特性。儘管將氧化亞銅沉積在吸附染料的二氧化鈦上還未完成，現在對於氧化亞銅/二氧化鈦塊材異質接面的研究仍對我們未來研究有很大的幫助。基於這篇研究的結果，我們相信只要能夠將氧化亞銅應用在染料敏化太陽能電池上，有著較佳長期使用穩定性的固態染料敏化太陽能電池就可以實現。

Characterization of Electrochemically Deposited Cu_2O/TiO_2 Bulk Hetero-Junction

Student：Wen-Peng Hsu　　　　　　　Advisors：Dr. Chao-Hsin Chien

Department of Electronics Engineering & Institute of Electronics
National Chiao Tung University

Abstract

Dye-sensitized solar cell (DSSC) is an attractive candidate for solar application owing to its properties of low cost and shorter payback time. But the leakage of electrolyte caused by the degradation of sealant is hard to avoid. To further improve the long term stability of DSSC, solid-state material may be a good substitute for liquid electrolyte layer. In this thesis, Cu_2O was used as a hole conductor and the Cu_2O/TiO_2 bulk hetero-junction is successfully formed.

In the beginning, the electrochemical deposition method is used to deposit the Cu_2O layer onto the nano-porous TiO_2 film. Since the deposition conditions are dependent on the surface properties of matter on which we deposited, it is not easy to find the best condition of deposition. As a result, material analysis plays an important role in the experiment. With the help of XPS and XRD analyses, we can find the best condition from variety of conditions. Besides, with the SEM technique, the deposition rate of material can be investigated. It is believed that all of the techniques of material analysis can help us to form the Cu_2O/TiO_2 bulk hetero-junction successfully.

Next, characteristics of the bulk hetero-junction are investigated with photo-electrical measurements and electrical impedance spectroscopy (EIS). With the results we obtained, it is

though that the recombination mechanism limits the performance of junctions. It is critical to inhibit the number of recombination centers before applying to DSSC. As a result, many conditions are tested in order to further eliminate the recombination current. With the EIS measurement, we can investigate the variation of recombination mechanism form its frequency response and then find the better way to improve the junction performance.

With the basic understanding of the bulk hetero-junction, some advanced measurements are performed to investigate the other characteristics of the junction. First, temperature dependence of junction is examined with the elevated temperatures. Second, optical condition of junctions is observed with different neutral density filters. Finally, the voltage response of junction is analyzed and the Mott-Schottky plot is obtained with the EIS results. With the Mott-Schottky result, the flat-band voltage is obtained and the complete model of band energy can be constructed.

In this thesis, the Cu_2O/TiO_2 bulk hetero-junction is form successfully with electrochemical deposition method and suitable deposition conditions. And the characteristics of the junction are investigated by the measurement of DC IV and AC EIS techniques. Although deposition of Cu_2O on dyed-TiO_2 is not accomplished, the research of Cu_2O/TiO_2 bulk hetero-junction now will be a good help in the future study. Based on this research, it is believed that solid-state DSSC with better long term stability can be achieved with application of Cu_2O material to DSSC.

誌謝

在這兩年的研究所生活中，由於有很多人的協助，才能讓我順利完成我目前的研究，非常感謝你們。首先要感謝我的指導老師簡昭欣教授，您在課業以及研究上給予我最大的協助，並適時地幫我們指點迷津，也教導我們待人處事的道理，更會不時關心我們的生活狀況，您是我研究所生活中的一大支柱。

其次要感謝實驗室的大家，明瑞學長、志彥學長、兆鈫學長、家豪學長、宇彥學長等各位實驗室學長，謝謝你們教我使用各種儀器設備，以及在專業知識上給予我適時援助，使我的研究能夠順利進展；政庭、宗佑、柏錡、耀陞各位同學，謝謝你們陪我度過研究所的生活，以及對於我課業跟研究方面上的幫忙，讓我在研究的路過程更加無往不利，才能有今日的成果。

再來要感謝提供我實驗中所使用器材的一些前輩，奈米中心的陳悅婷小姐、林聖欽先生、陳聯珠小姐等人，以及NDL的沈奕伶小姐、姚潔宜小姐、周棟煥先生、黃文賢先生等人，讓我做實驗的過程中沒有阻礙。張簡鵬崇學長、李美儀學姐，非常謝謝你們在電化學方面的協助以及指導，讓我的實驗跟量測可以順利完成。

另外在研究所的生活中，也要感謝別間實驗室同學們的幫忙以及照顧，除了課業上的切磋以及研究方面的討論外，還有課外上的活動，例如打球、聚餐等，都讓我的研究所生活增添了很多額外的樂趣，也讓我認識了更多的同學。有了這麼多同學的陪伴以及鼓勵，讓我的研究所生活更加多采多姿。

最後，我要感謝在我的人生以及求學的路上全心全力支持我的父母，沒有你們對我的細心呵護以及辛苦拉拔，我也不會有今日的成就。真的很感謝你們在求學路上對我的支持，你們是我經濟跟精神上最強大的後盾，讓我沒有後顧之憂地專注在我的學業上。在未來的日子裡，你們永遠是我的支柱，謝謝你們！

Contents

Chapter 4 Junction Characterizations

Table Cptions

Figure Captions

Chapter 1 Introduction

Chapter 2 Experimental Methods

Chapter 3 Electrochemical Deposition and Material Analysis

Chapter 4 Junction Characterizations

Chapter 5 Advanced measurements

Chapter 1
Introduction

The demand of energy grows up very rapidly in recent years. Nearly everything that can make our life convenient is energy consuming, for example, machines, vehicles and electrical equipments. Although there are so many ways to produce energy, it is always insufficient and polluted. For instance, one of the major methods is the direct burning of fossil fuel, which can make serious air pollution by discharging carbon oxide and carbon dioxide. Except fossil fuel, nuclear power may be a more efficient way to produce energy, but it is very difficult to handle the nuclear waste. In the present, low pollutant producing, source abundant and non-expensive are the basic requirements for the new era energy. To produce energy sufficiently but not destroying our environment is an urgent issue.

One of the possible technologies for energy is the solar cell, which is a device that converting energy of sunlight to electricity directly. For the abundance, inexhaustibility of solar energy, and the least pollution production in the operation of solar cells, the photovoltaic device is a promising candidate for energy production in the future.

The working principle of the conventional solar cell is based on the properties of a p-n junction structure. Incident photons interact with electrons in the semiconductor bulk and cause the excitation of electrons to the conduction band. The build-in potential in the depletion region of the p-n junction causes separation of electrons in the conduction band and holes in the valence band. When electrons and holes are separated and drifted out of depletion region, each one will transport to corresponding electrode by diffusion because of the concentration gradient induced in the bulk material. Briefly speaking, the operation of a solar cell includes three major stages, absorption separation and transportation.

Although it is possible to attain sufficiently high light conversion efficiency in conventional semiconductor p-n junction structures, the contrary high cost in material purification limits the payback time seriously. The other disadvantage of silicon solar cells is the use of toxic chemicals in manufacture. To obtain a photovoltaic component better in terrestrial use, new architecture with less material consuming is required. The remarkable energy conversion efficiency achieved in dye-sensitized solar cell (DSSC) has demonstrated the possibility to gain high photovoltaic performance in relatively low material cost with a different solar energy harvesting architecture. Table1.1 [1, 2] are lists of the energy payback time of different solar cells; it is obvious that the payback time for DSSC is much shorter than other solar cells; just as mentioned before.

Dye sensitized solar cell, proposed by M.Grätzel at 1991 [3], works different from conventional structures. The basic structure of the device is shown as Fig.1.1 [4], the specially designed dye molecule, as the major light absorber, are on one side chemically absorbed on the surface of titanium dioxide deposited on TCO (transparent conducting oxide) glass substrate while the other side is immersed in I^- / I_3^- electrolyte with catalytic Pt or carbon layer as the counter electrode. Upon light absorption from TCO side, the electron at the ground state of the dye is excited to the excited states. After that, the electron in the excited state inject ultra fast to the conduction band of TiO_2. The injected electrons will diffuse in the TiO_2 layer due to the concentration gradient before reaching the anode of the cell. The left hole in the ground state of dye will be reduced by I^- / I_3^- ionic electrolyte.

However, there are severe problems for present DSSCs such as solvent evaporation, dye degradation, and seal imperfection in the encapsulation of liquid electrolyte in these cells. Several solid state materials are proposed to replace the liquid redox electrolyte to solve these problems that limited the efficiency of dye-sensitized solar cells. For example, RT molten salts [5], conducting organic polymer [6], polymer gel electrolyte [7] and p-type semiconductors [8] are suitable as hole conductor in cells. There are some criteria for these materials, such as transparency in visible spectrum, good conductivity to hole, and proper method to deposit in the nano-porous TiO_2 structure. The basic structure of solid-state DSSC is shown in Fig.1.2 [9], it is similar to liquid DSSC except for the replace of liquid electrolyte to solid-state material.

Since the TiO2 thickness for DSSC should be over several micrometers, there are not many suitable processes to deposit the hole conductor on the nano-porous film to form the hetero-junction well. Solvent removal method and the electrochemical deposition method are the two common ways to fill the pores of the TiO_2.

Solvent removal method is a way that a p-type semiconductor is usually dissolved in a suitable solvent and filled into nano-porous TiO_2 film by dipcoating or spicoating. After that, the sample was heated to evaporate the solvent. It is a relatively easy way to deposit materials such as CuSCN [10], CuI [11], and spiro-OMeTAD [12], and the performance of solid-state DSSC used these materials are already demonstrated. However, forming a good contact with the dyed TiO_2 particles by this method is very hard since dye may detach from the TiO_2 surface in deposition process, and lead to the low efficiency of solid-state DSSCs.

Electrochemical deposition method is normally more material restricted and is dependent on both the characteristics of deposited material and the surface properties of the material on which it is deposited. Therefore, if we want to fill the porous structure well, the best deposition condition must be found. For example, it has been showed the growth of $CuInSe_2$ within porous TiO_2 was controllable by using modified electrolyte compositions [13]. Besides, CuSCN was already reported to be electrochemically deposited onto dye adsorbed ZnO by this method and the efficiency was 1.5% [14], and it was also deposited onto TiO_2 nano-crystalline surface with demonstrating p-n hetero-junction characteristics [15,16].

Cuprous oxide (Cu_2O) is an appropriate p-type material in solar energy application because it is direct band gap, abundant in element on the earth, and is non-toxic. Although Cu_2O should be applicable as a rarely existed intrinsic p-type binary oxide, the preparation methods highly limited its use. Direct oxidation of copper metal cannot be applied to other substrates. In spite of oxidation, another method was proposed to deposit Cu_2O nano-particle onto ZnO nanowire, and the photovoltaic characteristics are observed on the all oxide composed hetero-junction [17]. However, the reported ZnO thickness with this method was still less than 3 um.

In this thesis, we have applied he electrochemical deposition method to directly deposit Cu_2O onto nano-porous TiO_2 film. By applying appropriate constant current level, we were able to control the growth rate of Cu_2O within the nano-porous network and Cu_2O was successfully filled the TiO_2, which its thickness is more than $5\mu m$. Most important of all, the whole fabrication flow is quite simple and is environmentally benign. The measured electrical characteristics of this all oxide composed hetero-junction had shown the similar behavior with the conventional p-n junctions. By applying different measurement techniques we explored the preliminary knowledge about this bulk hetero-junction composed by two wide band-gap oxides.

Table 1.1

Cell Technology	Energy Payback Time (EPBT) (yr)
Single-crystal silicon	2.7
Non-ribbon multicrystalline silicon	2.2
Ribbon multicrystalline silicon	1.7
Cadmium telluride	1.0
Dye sensitized solar cell [8]	0.8

Table 1.1 Energy payback time of different type solar cells. [1, 2]

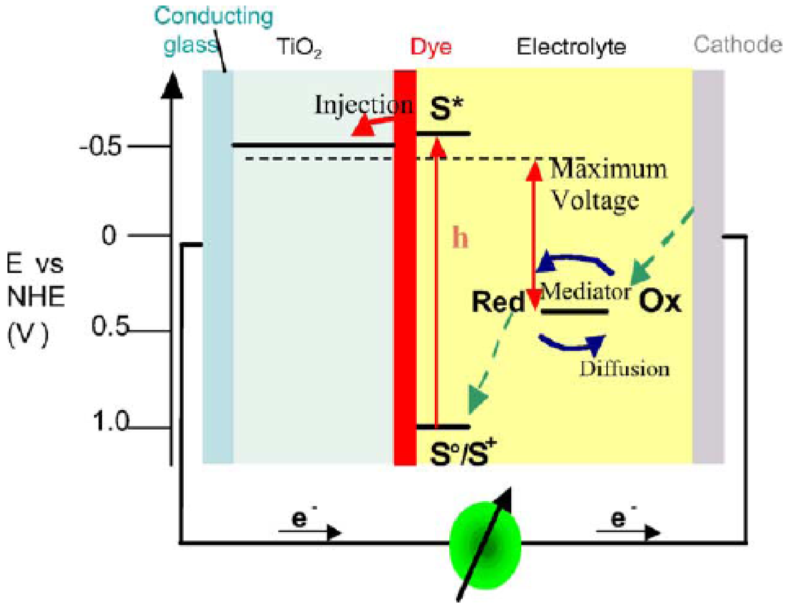

Fig.1.1 Basic structure of DSSC. [4]

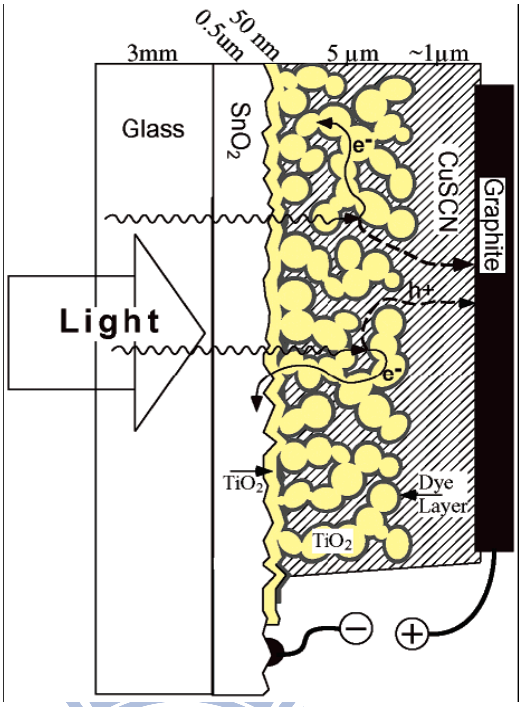

Fig.1.2 Basic structure of solid-state DSSC. [9]

Chapter 2
Experimental Methods

2.1 Materials and equipments used in fabrication

Used materials and chemicals

Substrate	
Glass/ITO	7 Ω/□
Glass/FTO	10 Ω/□
Glass/FTO	20 Ω/□
Glass/FTO	30 Ω/□
TiO_2 nano-crystalline powder	
TiO_2 P25	Degussa
Ingredient of TiO_2 paste	
Alpha terpineol	SHOWA
Ethyl cellulose	SHOWA
Acetic acid	SHOWA
Chemicals of electrochemical deposition	
Cupric sulphate	SHOWA
Lactic acid	SHOWA
Sodium hydroxide	SHOWA

Equipments in device fabrication

Microprocessor pH Meter	(SUNTEX SP-2200)
Atmospheric Anneal Furnace	(KH Union Co., Ltd)
Backend Vacuum Annealing Furnace	(Best Champion Technology Co., Ltd)
Sputtering System	(Ion Tech Microvac 450CB)
E-gun Evaporator	(ULVAC EBX-8C)

2.2 Equipments for characterization of materials

Surface Profiler	(Dektak 3030)
Scanning Electron Microscope	(Hitachi S-4000)
High-Resolution Scanning Electron Microscope & Energy Dispersive Spectrometer	(Hitachi S-4700I)
X-Ray Diffractometer	(PANalytical X'Pert Pro (MRD))
AES & ESCA	(VG Scientific Microlab 310F)

2.3 Electrochemical deposition experiments

Electrochemical deposition is an attractive method for preparing a variety of materials. It offers the advantages of low cost and high purity. A wide range of oxide semiconductors such as TiO_2 [18], ZnO [19], and CdO [20] were also synthesized by this method. Besides, there are many studies on electrochemical deposition of Cu_2O films [21-28]. The Cu_2O film can be synthesized in a three-electrode system containing $CuSO_4$-based aqueous solution by two kinds of methods - galvanostatic method and potentiostatic method.

For the application to solid-state DSSC, it is necessary to find the best condition to fill the porous TiO_2 well to for a good contact. Even for the static current condition, it was not always possible to obtain a fully filled bulk hetero-junction; similar to the electrochemical deposition of $CuInSe_2$ onto TiO_2 nano-particle or nano-tube proposed before [28], it was observed that the applied condition apparently influenced the pore-filling ability. With different conditions, we can achieve the different deposition mechanism, which is related to the ambipolar diffusion of ions with the nano-porous films.

2.4 Photo-electrical measurements

2.4.1 Current-voltage (I-V) measurement

The basic I-V measurement included two parts - the light source and the electrical measuring system. The solar simulator consists of Newport Oriel 96000 150W Xe lamp and AM1.5G filter 81094; the optical power of incident light was measured by the thermopile detector 818P-010-12 and calibrated to 100mW/cm^2 before measuring. The electrochemical potentiostat / galvanostat EG&G model 273A was connected to the device in two probing modes to characterize the I-V properties.

2.4.2 Electrical impedance spectroscopy (EIS) [29- 31]

The setup of EIS measurement was basically the same as the I-V measurement system, except that EG&G model 1025 Frequency Response Detector was connected to the electrochemical potentiostat / galvanostat EG&G model 273A. In the EIS measurement, small voltage oscillation signals with constant amplitude and different frequencies $V_0 e^{i\omega t}$ were applied, and the corresponding current responses $I(\omega)e^{i(\omega t+\varphi)}$ were analyzed. Then the impedance $Z(\omega) = \frac{V_0 e^{i\omega t}}{I(\omega)e^{i(\omega t+\varphi)}} = Z_0(\omega)e^{i\varphi}$, where φ is the phase difference, can be acquired. Electrical impedance spectroscopy measures the variation of impedance at different frequencies, so it is a trace of the variation of the impedance of measured sample.

Normally, the measurement for DSSC was done under the standard illumination with DC bias applied. The value of the DC bias was selected to be the open-circuit voltage of the measured device so that the device was under the static condition, i.e. there was almost no DC current when the measurement was proceeding. If not specially claimed, the conditions for EIS measurement in the experiment were always that the AC amplitude was of 5mV descending from 500 kHz to 0.01 Hz and DC bias equaled to open-circuit voltage.

Chapter 3
Electrochemical Deposition and Material Analysis

The reason of why we want to fabricate solid-state DSSC had been introduced in chapter1. Electrochemical deposition method seems to be a good way to deposit Cu_2O on the surface of nano-porous TiO_2 film to form a bulk hetero-junction. However, the best condition of electrochemical deposition must be found before using Cu_2O as a hole collector. In this chapter, the details of deposition condition and related material analyses are examined. All these results can help us to not only find the best condition for Cu_2O deposition but also understand the properties of Cu_2O with different deposition condition. It can provide the meaningful reference to the later works.

3.1 Deposition conditions

3.1.1 Cu_2O deposition mechanism

The possible reaction during Cu_2O deposition can be described by the following equations:

$$2Cu^{2+} + 2e^{-1} + 2OH^{-} \rightarrow Cu_2O + H_2O \qquad (1)$$

$$Cu^{2+} + 2e^{-1} \rightarrow Cu \qquad (2)$$

$$Cu_2O + 2e^{-1} + 2H^{+} \rightarrow 2Cu + H_2O \qquad (3)$$

It is obvious that equation (1) and equation (3) are pH dependent, at lower bath pH value the metallic Cu may form according to reaction(3). The films deposited at pH 7 is a compisite of Cu_2O and Cu; while the film deposite at bath pH value larger than 9 is pure Cu_2O. It means that with higher OH^- concentration the Cu_2O could be deposited easily. Besides, with the the the bath pH increased from 9 to 13, the prefered Cu_2O orientation also changed from (200) to (111). And all the results mentioned above corredponded to the previously proposed paper [32, 33]. According to these results discussed before, it is obvious that the pH value of solution is an important factor in the synthesis of Cu_2O.

3.1.2 Cu_2O Deposition methods

To electrochemically deposit Cu_2O onto the TiO_2 nano-particle, the solution was referenced to previously proposed one [21]: 0.4M cupric sulphate, 3M lactic acid, and sodium hydroxide was added to modify the pH value. The deposition was carried out at the set temperature in the standard three electrode configuration, as shown in Fig.3.1, Ag/AgCl be the reference electrode whereas Pt be the counter electrode, and the applied bias were controlled by the potentiostat.

Two types of electrochemical deposition methods, galvanostatic method and potentiostatic method, were both examined in our experiment. Fig.3.2. (a) shows the monitored deposition voltage profiles at constant current level. The voltage drastically change at the early initial stage and afterward became neatly steady for each deposition processes. It is easy to control the deposited Cu_2O thickness by the static deposition rate estimated from galvanostatic method. Compared with it, the potentiostatic method with constant voltage level shows the time dependent deposition current profiles, as shown in Fig.3.2 (b); and it is hard for us to control the deposition process.

3.1.3 Cu_2O deposition conditions

Even with the current static approach, a fully filled BHJ was not always accomplished; similar to the previously proposed electrochemical deposition of $CuInSe_2$ onto TiO_2 nano-particle or nano-tube [13], the applied pH value of solution (solution composition) did influence the pore-filling ability of the deposited material.

Fig.3.3 (a) shows the voltage profiles in bath solution with pH10, it is shown that the spontaneous potential oscillation is observed. It is a normal phenomenon in the alkaline Cu(II)/taetrate and lactate system when applying current level to electrochemical deposition [36, 37], and was caused by the variations in pH close to the electrode surface during the oscillation process. When spontaneous potential oscillation is observed, both Cu and Cu_2O are deposited. The oscillation period is effected by pH value and temperature. Besides, the current density also decides when the oscillation happened. A high current density favors Cu deposition and a low current density favors Cu_2O deposition. As shown in fig.3.3 (a), we can get static deposition voltage when the applying current density is lower enough. Fig.3.3 (b) shows the voltage profiles with different pH value but the same current level ($28\mu A/0.09cm^2$). As the pH increased, the voltage shifted to more negative value, which was due to the pH dependent deposition mechanism.

Although we can get static deposition rate with lower enough current density in solution with pH10, the deposition rate is too low to fill the nano-porous TiO_2 film. Beside, instead of plainly cumulative deposition from the bottom to the top, the Cu_2O also appeared on the top portion of nano-porous TiO_2; therefore, the formation of a complete bulk hetero-junction cannot be achieved, as shown in Fig.3.4. As a result, we use the solution with higher pH value, which we can apply the higher current density and hence get higher deposition rate.

Fig.3.5 shows the voltage profiles at different current levels at solution with pH10. We found that the magnitude of voltage was closely related to the applied current level; larger current level, higher voltage and Cu_2O deposition rate were observed if all the other deposition conditions were kept the same. In addition, different substrates did not lead to different results. This is due to the presence of an intentionally deposited condensed TiO_2 layer on top of the substrates, which could prevent the formation of reversed leakage path and shunt resistance lowering arising from the direct contact of Cu_2O with the substrates. As a result, negligible difference in the deposition can be anticipated if the distinct substrates had similar sheet resistance. This result also helped us justify whether or not the Cu_2O/TCO junction was formed. If there was unwanted great shunt leakage paths in the complete structure, it will become an ohmic junction instead of a rectified junction. Fig.3.6 shows the cross sectional SEM images of the film deposited with pH 14. The growth of Cu_2O starting from the bottom of TiO_2 was obviously observed, and the growth rate was found to be nearly constant and around 20nm/min.

3.2 Material Analyses

Once a well filled junction was obtained, the material analyses are needed to be conducted in order to characterize the physical properties of the deposited film. Fig.3.7 shows the XPS and XRD results of the sample prepared with $300\mu A/cm^2$ for 2 hours with 1.5μm porous TiO_2 and 20nm sputtered TiO_2 barrier layer on the ITO substrate. Three different pH values, 12.9, 14, and 14.7, are adapted as the solution pH value. From the Cu 2p spectra in Fig.3.7 (a), the peaks for Cu $2p_{1/2}$ and Cu $2p_{3/2}$ locate at

952.0eV and 932eV respectively, which agree well with the reported values for the cuprous oxide [38,39], and the CuO-related shake satellites were weak for samples with pH12.9 and pH14. We noted that when pH value reaches to 14.7, the obvious CuO-related shake satellites appear. Under this condition, we cannot get pure Cu_2O film. From the XRD diffraction spectra in Fig.3.7 (b), we obviously observed the major Cu_2O crystalline peaks without Cu or CuO peaks appearing. Besides, the sample with pH14 shows the strongest dominant Cu_2O (111) orientation. The TiO_2 anatase peak of the host layer below Cu_2O also could be found in the spectra, the rutile phase of P25, however, was relatively weak so that this phase was not be easily identified in the figure.

Fig.3.8 shows the XPS and XRD results at pH14 for 2 hours with different current level ranges from 40μA/cm^2 to 400μA/cm^2. For samples with current density of 40μA/cm^2, 80μA/cm^2 and 200μA/cm^2, the CuO-related shake satellites were very obvious in Fig.3.8 (a). And their XRD results in Fig.3.8 (b) showed weak Cu_2O orientation, which corresponded to the XPS results. Samples with current densities of 300μA/cm^2 and 400μA/cm^2 showed the Cu_2O characteristics in the XPS results. Therefore, their dominant Cu_2O (111) orientation is obviously strong. Even through, the (111) orientation of sample with 300μA/cm^2 was larger than the 400μA/cm^2 one.

As a result, from the XPS and XRD result discussed before, the deposition conditions with pH12.9 or pH14 and current density of 300μA/cm^2 may be the best condition to deposit pure Cu_2O on the nano-porous TiO_2 films.

According to the previously proposed paper [40], vacuum annealing of CuO bulk can make the surface of CuO bulk transform to Cu_2O by decreasing the contaminant of oxygen. And the experiment result was verified by the XPS spectrum. In the thesis, vacuum annealing is also applied in an attempt to get purer Cu_2O composition. Fig.3.9 shows the XPS and XRD results at 300μA/cm^2 and pH14 for 2 hours with different vacuum annealing conditions. All samples are heating in about 5e-7 torr for 15 minutes with different temperatures. It makes no difference in the condition of 100℃ to 300℃ at vacuum except for 300℃ in 0.3torr N2, in which the CuO component become a little larger.

In order to calculate the deposition rate, we deposit the Cu_2O film with different time and use the SEM technique to investigate its cross-sections and top-views. Fig.3.10 shows the SEM images, it was shown that Cu_2O growth from bottom layer of nano-porous TiO_2 to its upper layer, and the thickness of Cu_2O were about 300nm, 600nm, and 3000nm for deposition time of 15 minutes, 30 minutes, and 150 minutes, respectively. And the deposition rate was about 20nm/minutes. Besides, with longer deposition time, the number of Cu_2O grains on the surface of nano-porous also becomes larger.

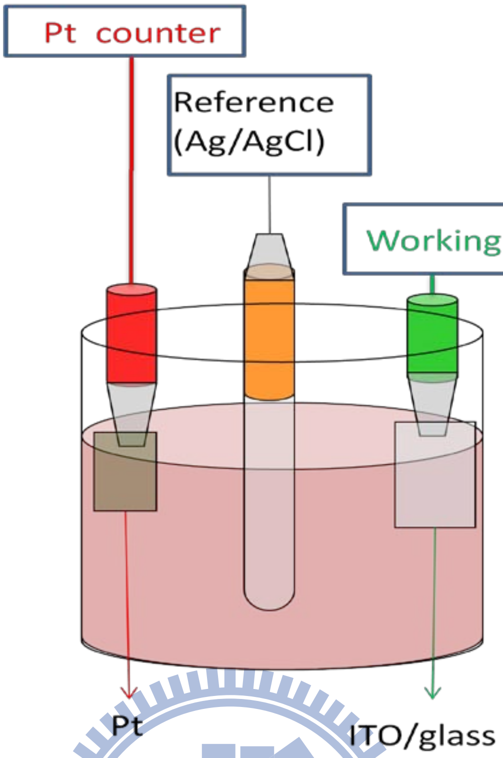

Fig.3.1 Equipment of electrochemical deposition.

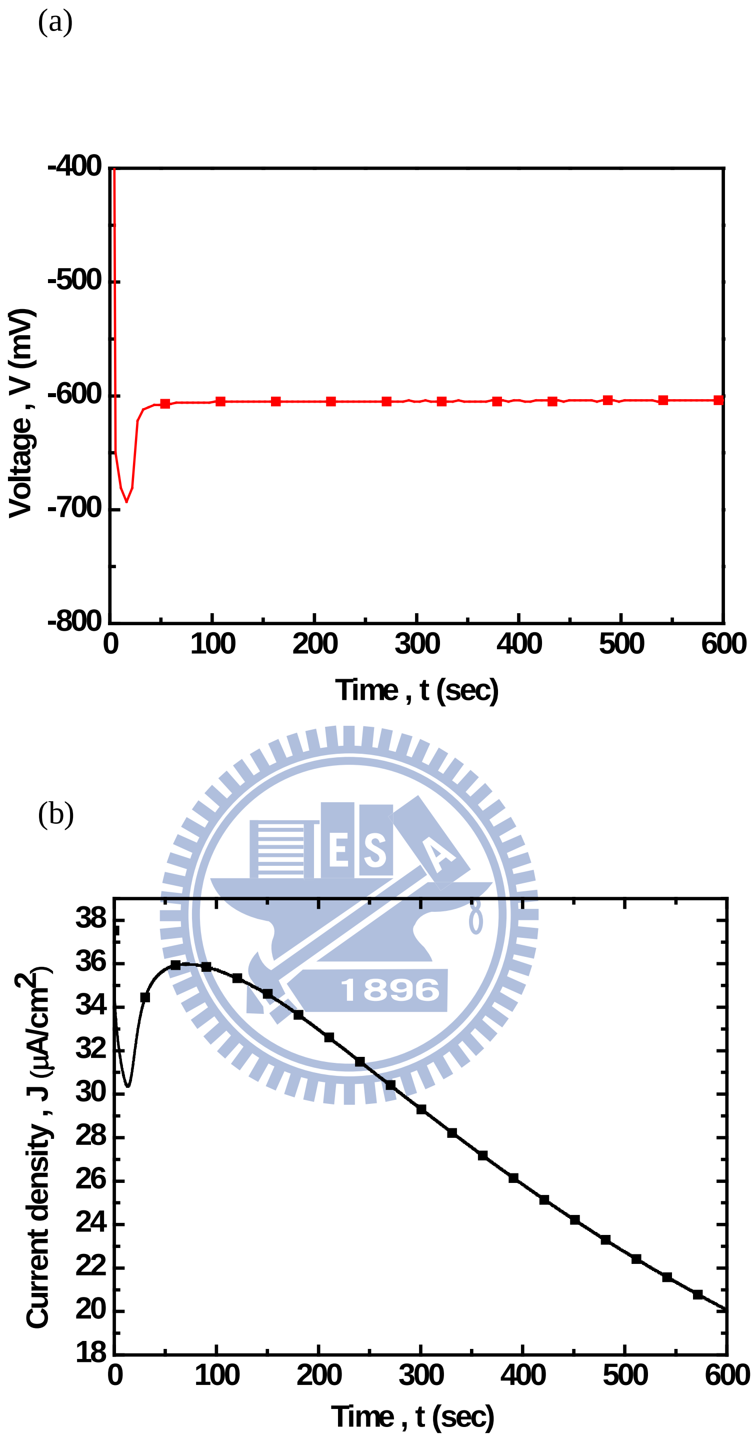

Fig.3.2 Deposition curve of two kinds of methods: (a) galvanostatic method, and (b) potentiostatic method.

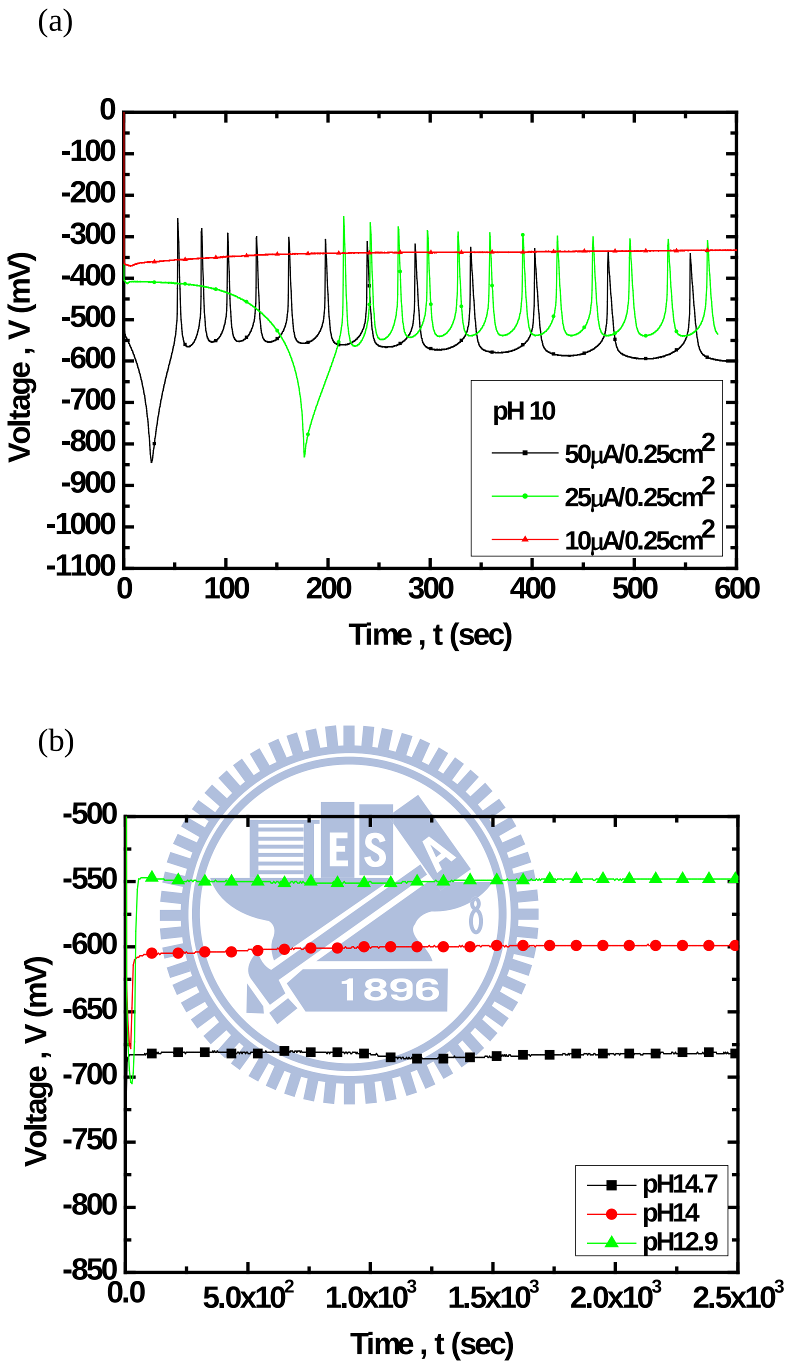

Fig.3.3 (a) Voltage profiles with different deposition current density in bath solution with pH 10.

(b) Voltage profiles with different current pH value at the current density of 10μA/0.25cm^2.

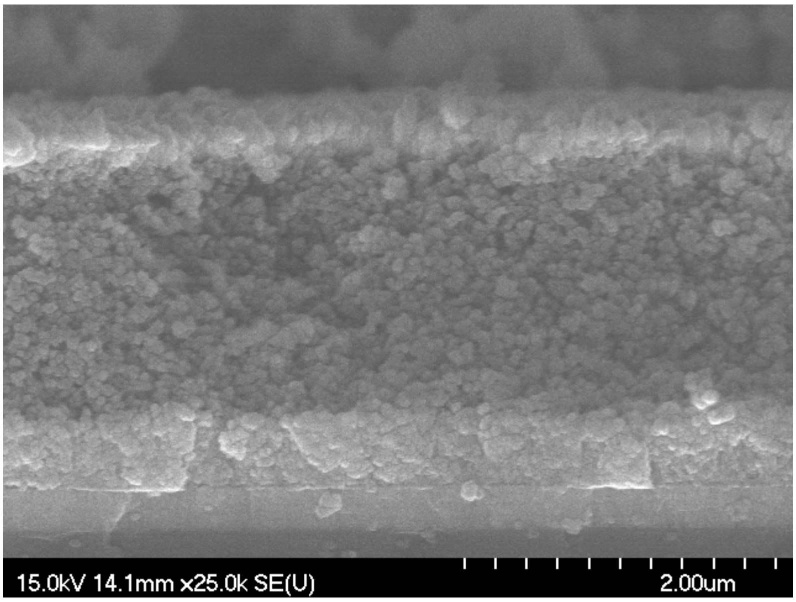

Fig.3.4 SEM images of as depositing nano-porous samples at 10μA/0.25 cm^2 for 6 hours (pH 10), and the identified Cu_2O regions were indicated in the figures.

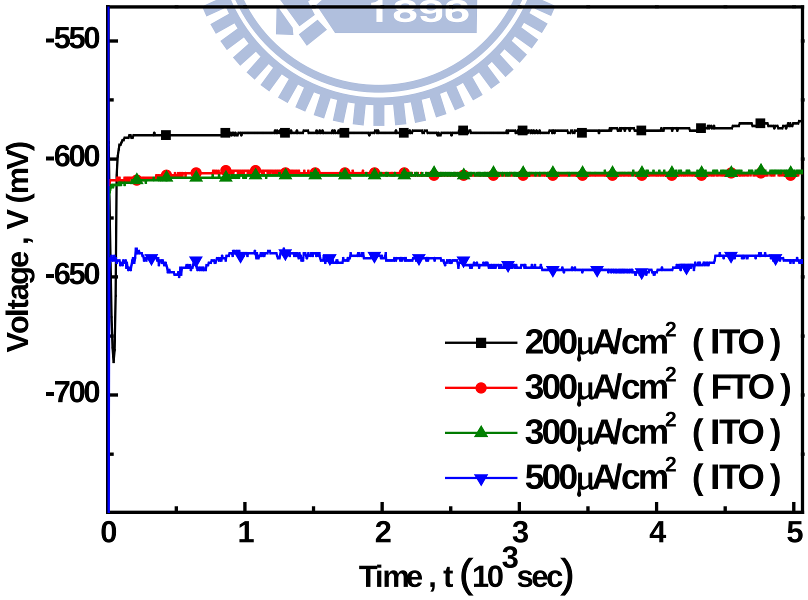

Fig.3.5 The voltage-time variations at different current levels with samples of P25 TiO_2, 20nm TiO_2 thin film, and the selected substrates, (1) 200μA/cm^2 ITO, (2) 300μA/cm^2 FTO, (3) 300μA/cm^2 ITO, and (4) 500μA/cm^2ITO.

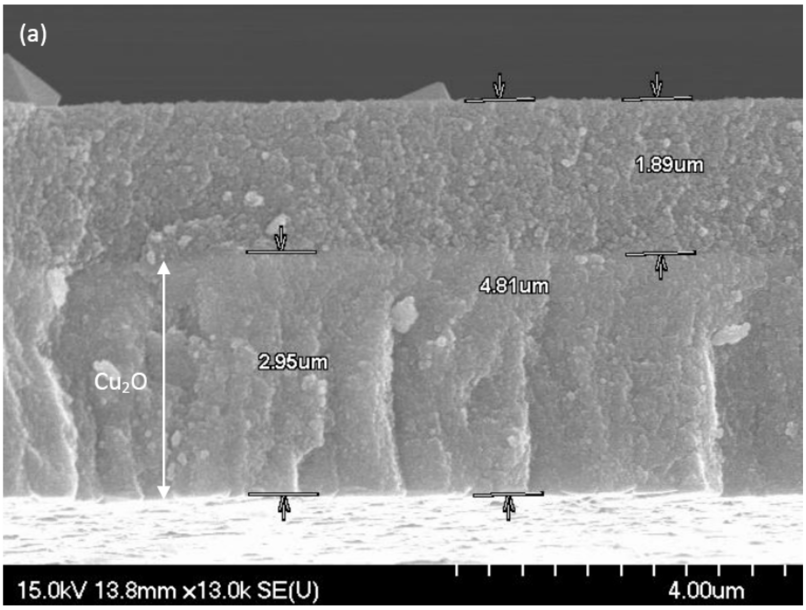

Fig3.6 SEM images of as depositing nano-porous samples at current density 300μA/cm^2 for 6 hours (pH 14), and the identified Cu_2O regions were indicated in the figures.

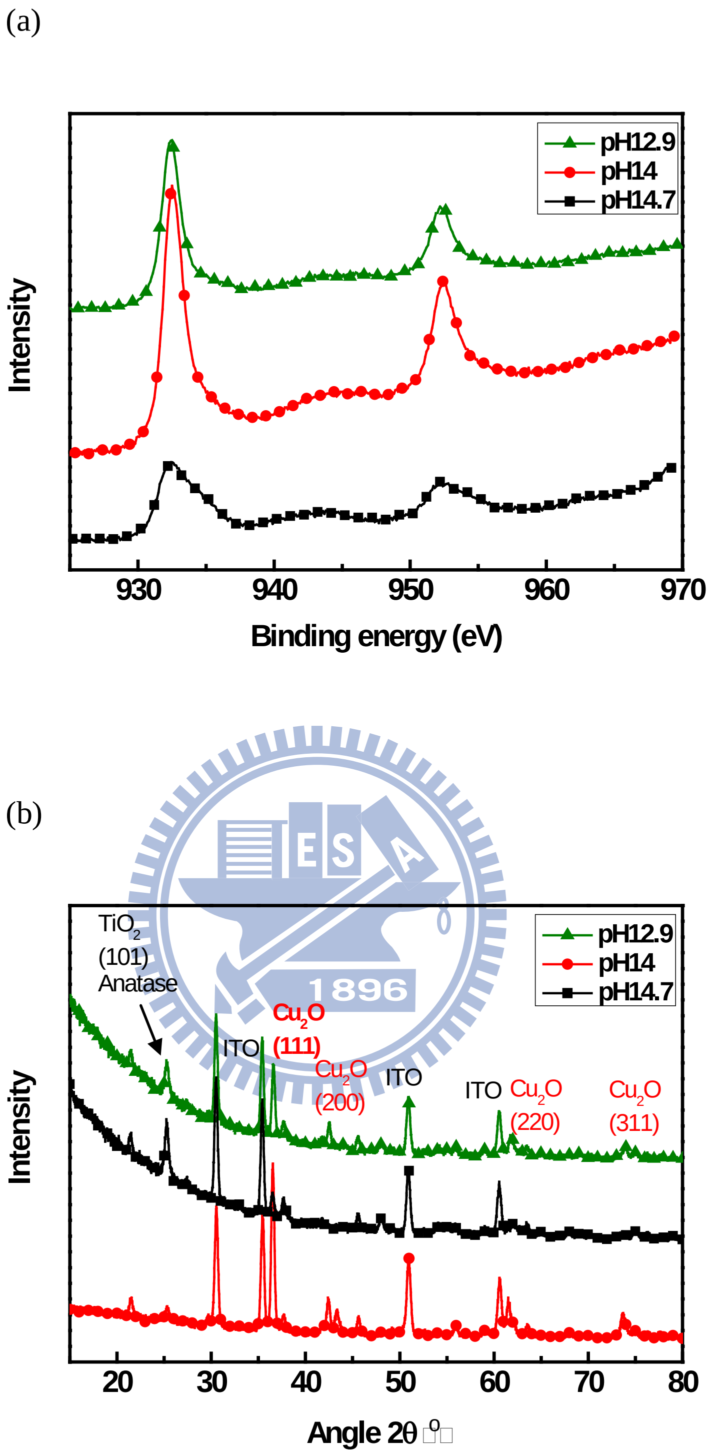

Fig.3.7 The (a) XPS, and (b) XRD results at deposition current density of $300\mu A/cm^2$ for 2 hours with different pH values of (1) pH12.8, (2) pH14, and (3) pH14.7.

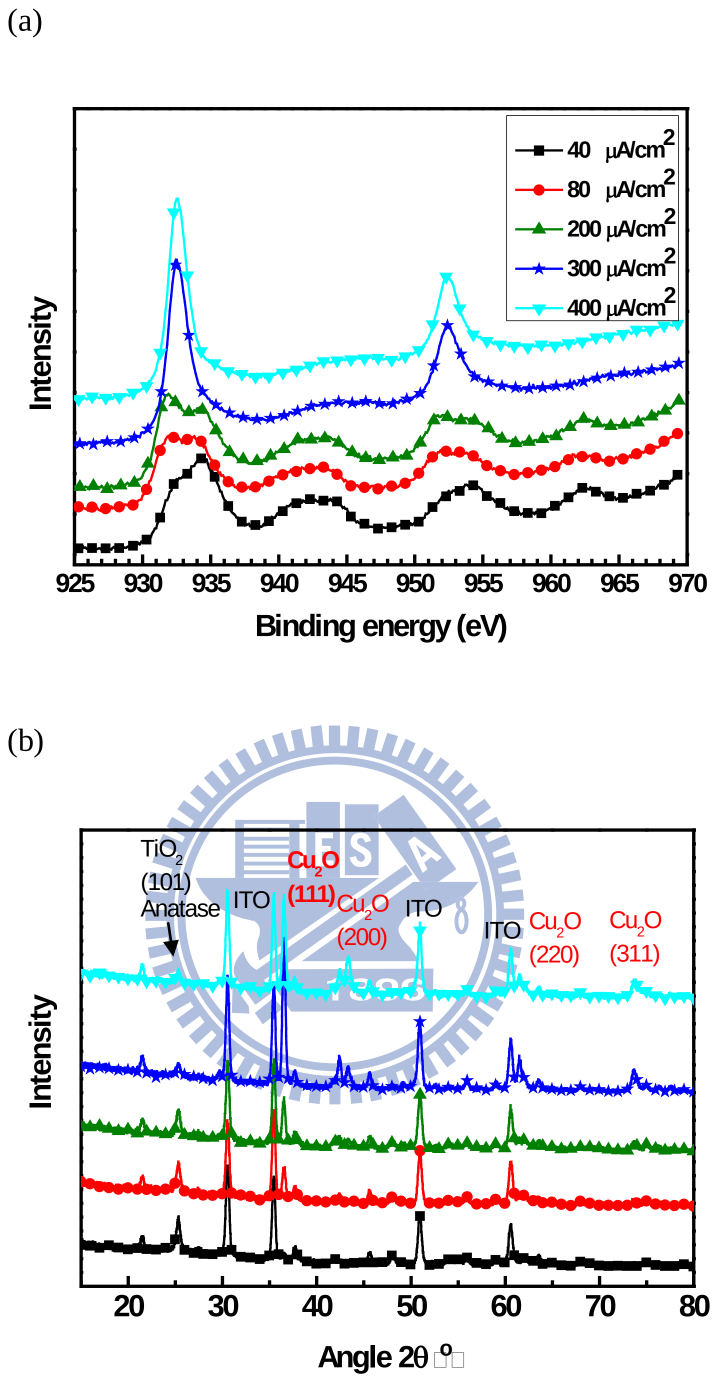

Fig.3.8 The (a) XPS and (b) XRD results at bath solution with pH14 for 2 hours at different current levels of (1) 40µA/cm^2, (2) 80µA/cm^2, (3) 200µA/cm^2, (4) 300µA/cm^2, and (5) 400µA/cm^2.

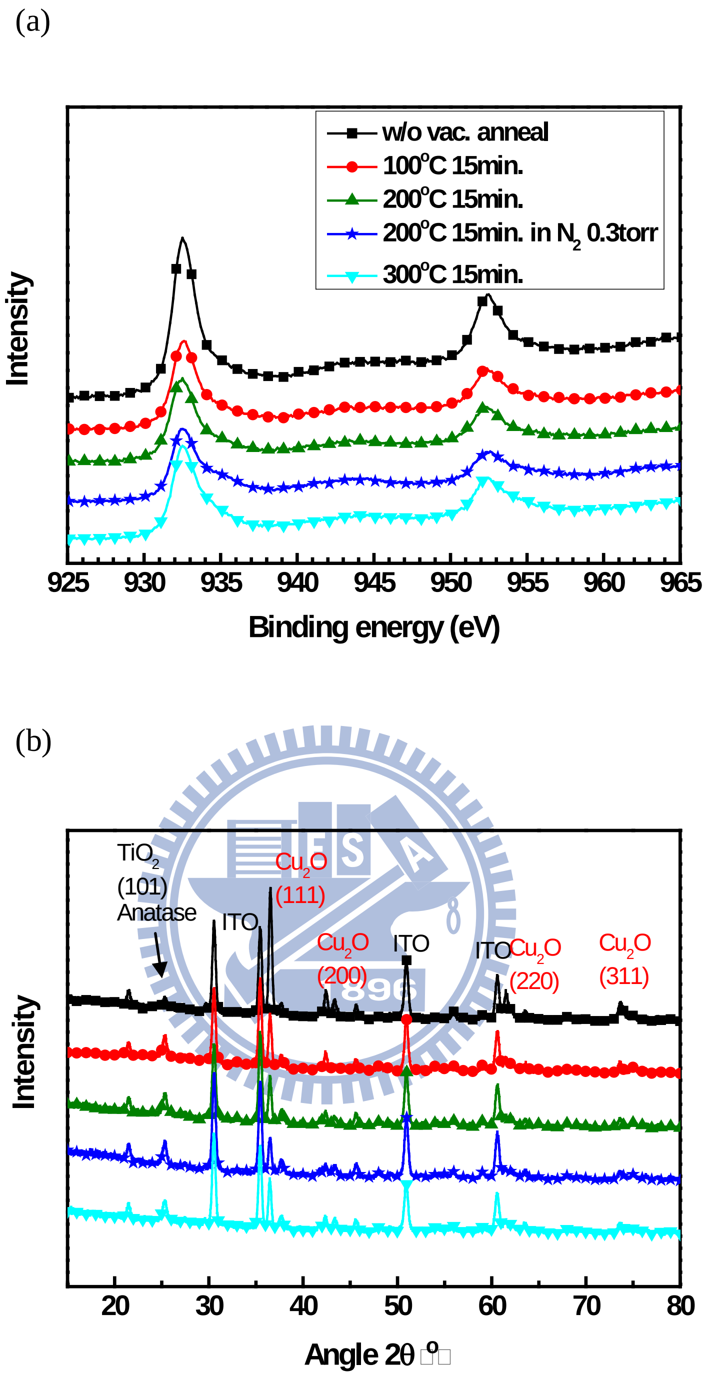

Fig.3.9 The (a) XPS and (b) XRD results at current density of 300μA/cm^2 and bath solution with pH14 for 2 hours at different vacuum annealing conditions of (1) w/o annealing, (2) 100℃ 15minutes, (3) 200℃ 15minutes, (4) 200℃ 15minutes in N2 0.3 torr, and (5) 300℃ 15 minutes.

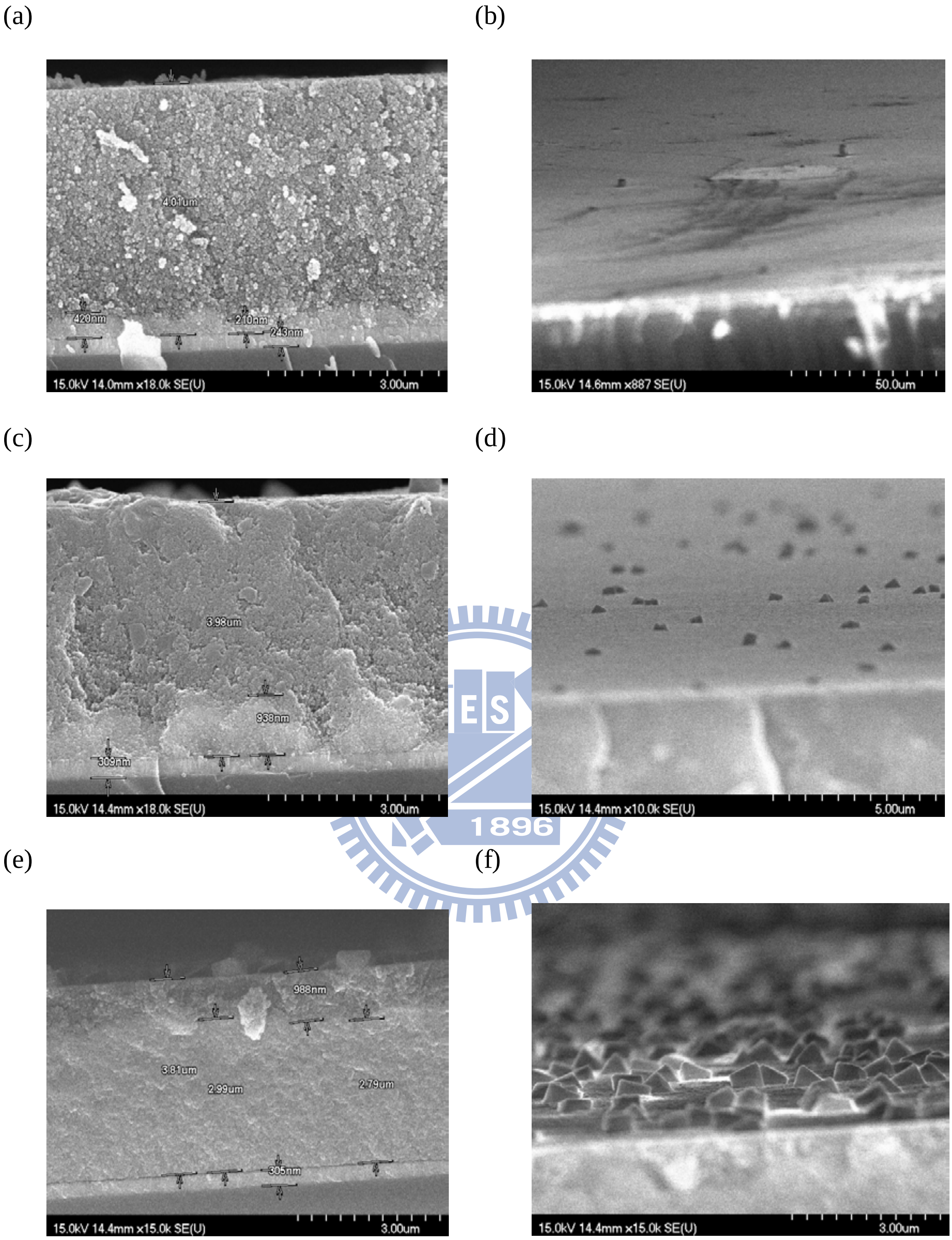

Fig.3.10 SEM cross-sections and top views with different deposition time of (a)(b) 15 minutes, (c)(d) 30 minutes, (e)(f) 150 minutes.

Chapter 4
Junction Characterizations

Based on previous results, we find the better conditions for Cu_2O deposition and have the basic understanding of material characteristics. In this chapter, we successfully fabricate the Cu_2O bulk hetero-junction and investigate its characteristics by electrical measurements. With the study of the obtained results, we can comprehend the basic characteristics of the junction and compare it with the properties of conventional p-n junction. Furthermore, we acquire the frequency response by applying electrochemical impedance spectroscopy (EIS) under different conditions to get the information about charge diffusion and recombination mechanism inside the structure.

4.1 Fabrication process

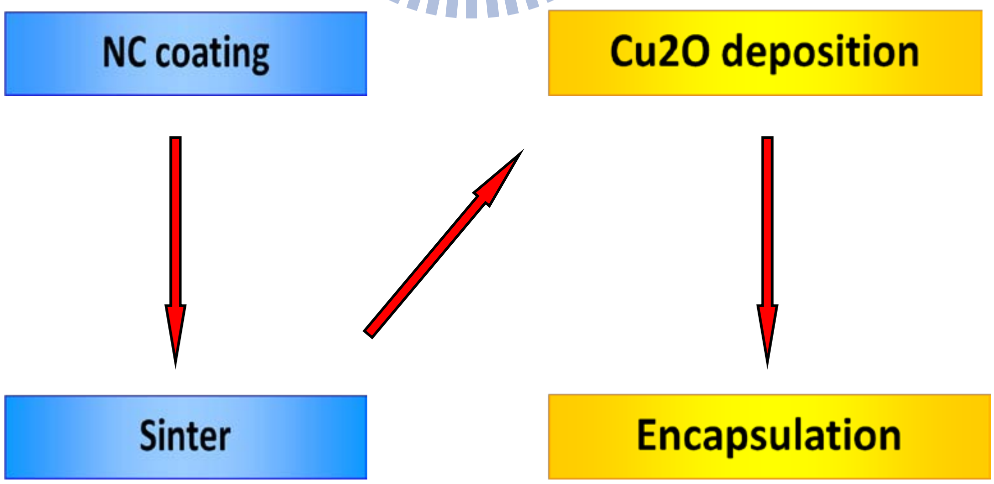

Fig.4.1 Fabrication flow of Cu_2O/TiO_2 bulk hetero-junction.

The fabrication flow is depicted as Fig.4.1. In the beginning, the TCO (20Ω/□ FTO or 10Ω/□ ITO) glasses were ultrasonically cleaned in ethanol first and then in de-ionized water. 20nm amorphous thin film TiO_2 was reactively sputtered onto the TCO substrate before the coating of TiO_2 nano-particles. The preparation of TiO_2 paste was referenced to the previous method [41]; the paste was coated on TCO glass substrate by the doctor blade method. After that, the TiO_2 film was sintered in atmospheric ambient at 450℃ for 2 hours with air flow. The thickness of the prepared TiO_2 was determined by Surface Profiler

For electrochemical deposition, the samples were immersed in the $CuSO_4$-based aqueous solution at room temperature; the solution consisted of 0.4M cupric sulfate and 3M lactic acid and the pH of the bath was adjusted by the addition of sodium hydroxide. The deposition was carried out at the set temperatures in the standard three electrode configuration, Ag/AgCl be the reference whereas Pt be the counter, and the applied bias were controlled by the potentiostat. After the 4 to 6 hours deposition, the reddish sample was moved out from the solution and rinsed by ethanol and water and was baked to remove residual solution on the surface.

For electrical measurement, 150nm Au contact pad was E-gun evaporated onto the Cu_2O surface; the complete $Au/Cu_2O/TiO_2/TCO$ junction structure is shown in Fig.4.2. Then junction properties were measured by the pontentiostat in two electrode configuration.

4.2 Photo-electrical analyses

4.2.1 Basic characteristics of junction

The current density of device with different deposition conditions under both forward and reverse bias is presented in Fig.4.3. The deposition current level we applied was of $50\mu A$ with active area $0.16cm^2$ for 4 hours on the $1.5\mu m$ P25 porous layer with 20nm TiO_2 barrier layer under it. Rectifying characteristic of the junctions was clearly observed, and both forward and reverse currents increased with the raise of measured temperature. It is similar to the conventional p-n junction.

Fig.4.4 (a) displays the I-V characteristics of junctions with different deposition conditions. All the three devices showed slope transition in the forward region as the conventional p-n junction did. The forward current densities differed most in the low voltage region. Besides, larger reverse current densities were obtained for junctions with larger current densities in low voltage region. So, the current in the low voltages region was postulated to be provided by the recombination centers, and these trap centers also acted as the dominant generation source of the reversed current. Even though the exact mechanism and the locations of these traps could not be clearly clarified by available data now, the amount of these centers should be related to the composition of Cu_2O for the different I-V characteristics with the different deposition conditions.

Fig.4.4 (b) is the optical responses of these junctions, and the highest photo-voltage and photocurrent achieved under 1 sun illumination were 0.38V and $0.21mA/cm^2$ for the device with the lowest recombination current. This result was consistent to our speculation of the effect by the Cu_2O bulk traps or Cu_2O/TiO_2

interface traps. Since the junction will be influenced by these traps, it is important to lower down the number of these recombination centers before applying to the DSSCs.

Fig.4.5 shows the impedance spectrums under zero bias of these junctions. There were no apparent difference of the impedance magnitude at higher frequency region, but the impedance magnitude deviated apparently at low frequency region. As a result, the dominant electron transfer mechanism around zero bias was via the interface or bulk trapping states. Noted that the characteristic frequencies for these samples were separated obviously, and the characteristic frequencies for these three samples were consistent with those exhibited in recombination current and impedance magnitude as well. Hence, the characteristic frequencies could be related to the recombination rate as in the conventional DSSC results [42]. It was reasonable that the device with lower characteristic frequency, which is related to the smaller recombination rate, shows better optical performance.

Based on the above experimental results and discussion, it was known the Cu_2O/TiO_2 bulk hetero-junction had certain similarities with a conventional p-n junction. With both DC I-V and AC EIS analyses, we could evaluate the recombination behavior of this 3D disordered junction. It was thought that the recombination behavior is the most important factor that limited the junction performance. Therefore, to comprehend the cause of the defects and then suppress the formation of these traps is the purpose we pursuing now.

4.2.2 Effect of other factors

In this section, we investigate the IV and EIS results with many groups of conditions. This help us to not only further understand the effect of different conditions but also find the best condition to achieve better device performance. If not specially claimed, the conditions for Cu_2O deposition are galvanostatic deposition method with current density $28\mu A/0.09cm^2$ for 6 hours in the $CuSO_4$-based aqueous solution with pH14.

First of all, Cu_2O was deposited on the TiO_2 layer with two sintering conditions, 375℃ for 2 hours and 450℃ for 3 hours. The deposition conditions were maintained the same for the two junctions and the substrates used were ITO for 375℃ 2 hours and FTO for 450℃ 3 hours. And the sheet resistances of the two substrates are the same (20Ω/□) after sintering. The dark current and photocurrent to voltage characteristics are shown in Fig.4.6 (a) and (b), respectively. It was obvious that the junction with TiO_2 sinter condition of 450℃ for 3 hours showed smaller recombination current and reverse current than the one with 375℃ for 2 hours; and the optical result also showed the larger photocurrent but nearly the same photo-voltage for junction with TiO_2 sinter condition of 450℃ for 3 hours. From the results, it seems that junction fabricated by TiO_2 film with sinter condition of 450℃ for 3 hours, which showed smaller recombination current and larger photocurrent, is a better condition. Fig.4.7 (a) and (b) displays the dark current and photocurrent characteristics of junctions with different substrates. Noted that the sinter conditions are 375℃ 2 hours and 450℃ 3 hours for the ITO and FTO substrates, respectively. Again, those junctions on FTO substrates, which TiO_2 sinter condition was 450℃ 3 hours, showed better performance. Besides, the photocurrent of junction fabricated on

FTO substrates with 10Ω/□ was larger since its sheet resistance is smaller than the 30Ω/□ one.

In Fig.4.8 (a) and (b), the EIS phase plot and Nyquist plot are presented. Although the Nyquist plot showed the same trace except for the impedance value, the peak frequencies which is related to recombination mechanism shifted to higher value for junctions with TiO_2 sinter condition of 450℃ 3 hours. It seems contradictory to the I-V characteristics shown before since the one with small recombination current showed larger peak frequency. But the TiO_2 sinter conditions are different for junctions fabricated on different substrates, so it is obvious that the divergence in peak frequency values is related to the TiO_2 surface properties. From the experiment results, although junctions with TiO_2 sinter condition of 450℃ 3 hours show higher peak frequency values, it is not related to the higher recombination currents. Besides, the high frequency circle in Nyquist is obvious, and we assume the circle is related to the Cu_2O/TiO_2 junction since the frequency range is reasonable.

Next, another experiment was performed to clarify whether the deposition time affect the electrical characteristics of junction. Basic I-V characteristics of these junctions are depicted in Fig.4.9 (a) and (b). The dark I-V curves were quite similar except for a little deviation in low voltage region, and the difference of recombination current is also due to this deviation. The optical characteristics displays that the junction with Cu_2O deposition time of 4 hours showed larger photo-voltage, which is related to its smaller recombination current in the dark I-V curves. Fig.4.10 (a) and (b) shows the EIS results of junctions with different Cu_2O deposition time, and it was found that these three junctions showed the similar impedance trace in Nyquist plot. It was noted that for junctions with longer Cu_2O deposition time, the peak frequencies shifted to lower values, which meant the improved recombination mechanism. It is believe that there is a repair mechanism between the Cu_2O/TiO_2 boundaries in the deposition process, and the junctions after repaired may showed better recombination characteristics. As a result, for samples with longer deposition time, the junctions will be repaired more and the numbers of recombination centers between the Cu_2O/TiO_2 junctions will be eliminated.

Third, for the further application to the DSSC, we examined the effect of the deposition mechanism after the TiO_2 layer was coated with dye. It is reasonable that the surface property with dye absorption is very different from surface without dye absorption, and the deposition condition will not be the same for different surface properties. Basic I-V characteristics of the devices with dye absorption are depicted in Fig.4.11 (a) and (b). It was shown that both the devices with dye absorption showed larger recombination currents and reverse currents. The optical characteristics also displayed the same results, which the devices with dye absorption showed the worse performance than those without dye absorption, especially the one with N3 dye. Besides, the deviation between the two dyed devices came from the different binding characteristics of dye with the TiO_2 surface. All the divergence of the I-V characteristics for these devices may be ascribed to the properties of TiO_2 surfaces, which is very different from each other. Hence, when we apply the same deposition condition on surfaces with different properties, the mechanism for deposition must be different. Furthermore, the detachment of dye which absorbed on the TiO_2 surface also affected the deposition mechanism. In order to confirm this postulation, EIS measurement is conducted and the results are presented in Fig.4.12. Fig.4.12 (a) shows the result of EIS phase, and it was found that the peak frequency, which corresponded to recombination mechanism, of devices with dye absorption shifted to higher value in phase plot. Fig.4.12 (b) displays the Nyquist plot, and it is apparent that the impedances of circles related to recombination mechanism also decreased with the increased values of peak frequencies in phase plot.

In the final part of the section, we applied the same deposition conditions in the solutions with different pH values in order to investigate the effect of deposition pH value. Fig.4.13 (a) and (b) displays the dark current and photocurrent to voltage characteristics of junctions with pH value of 14.7, 14, and 12.9. The junction with pH 14 showed the best I-V characteristic and the junction with pH 14.7 showed the worse characteristic which may be due to the change of composition as discussed before. It was also found that the junction with pH14.7 showed the worse characteristic and the other junctions showed the similar characteristics in the photocurrent to voltage results. The EIS characteristics of these junctions are also depicted in Fig.4.14 (a) and (b), it is obvious that junction with pH 14 showed the lowest peak frequency than others in the phase plot. Again, the junctions with pH14 and pH12.9 showed the similar trace in the Nyquist plot except for the magnitudes of impedance, and the result of junctions with pH14.7 is very different. From the results we investigated before, pH14 may be a better condition within the three pH values we used to deposit the Cu_2O films.

4.2.3 Effect of vacuum annealing

To achieve the best electrical characteristic, except for the request of deposition methods, the composition of p-type materials we deposited is also an important issue. As a result, high purity of p-type Cu_2O film is our purpose. In previously proposed paper [43], high vacuum treatment was adapted and the surface composition of CuO and Cu_2O was investigated by XPS and XAES. In our research, high vacuum anneal treatment was also applied in order to get the purer Cu_2O composition. The characteristics of junctions with different vacuum annealing treatments were discussed in this part.

Experiment was performed to investigate the effect of vacuum annealing temperature. Noted that the annealing pressure was about 5e-7 torr and the annealing time was 30 minutes. Fig.4.15 (a) are the dark current to voltage characteristics of junctions with different vacuum annealing temperatures, it was found that junctions with vacuum annealing treatment shows larger recombination currents than junctions without treatment except for the one with 300℃ annealing. Besides, the junction with 100℃ annealing showed similar diffusion current levels with the one without annealing, and both were larger than these two junctions with 200℃ annealing. Besides, for junctions with 200℃ vacuum annealing treatment, the one in N2 ambient (about 0.3 torr) showed worse performance than the other. Fig.4.15 (b) shows the photocurrent to voltage characteristics of these junctions with different vacuum annealing conditions, and it displayed the same trends that junctions with smaller recombination currents showed better optical performance. It is mentioned that the junctions with 300℃ annealing showed very small current levels both in forward and reverse bias regions, but the rectify characteristic was not investigated.

With the results we investigated, it seemed that vacuum annealing treatment cannot provide better performance. From the analysis of XPS results about different vacuum annealing conditions before, it was shown that the composition of deposited Cu_2O with 100℃, 200℃, and 300℃ vacuum annealing were nearly the same. So the deviation of these junctions cannot be ascribed to the change of Cu_2O composition. As a result, it is reasonable to postulate that the vacuum annealing treatment may break the junction and hence degrade the electrical characteristics.

In order to improve our postulation, EIS measurement was conducted, and the result is shown in Fig.4.16. Figt.4.16 (a) is the phase plot, it was found that junctions with higher vacuum annealing temperature showed lower peak frequencies values except for the 100℃ one, which showed a little larger value of peak frequency. The contradictory results of phase plot compared to the I-V characteristics can be explained by the destruction of Cu_2O/TiO_2 junctions. The recombination time, which is proportional to the reverse frequency, became smaller because the Cu_2O/TiO_2 junction was broken with the elevated temperatures. The Nyquist plot is also shown in Fig.4.16 (b) and (c), it is obvious that the circles related to the high frequency region became larger with the increase of annealing temperature. It may be reasonable to postulate the circles with high frequency region is related to the Cu_2O/TiO_2 junction since the composition and crystal phase of TiO_2 itself do not change in the annealing temperature range.

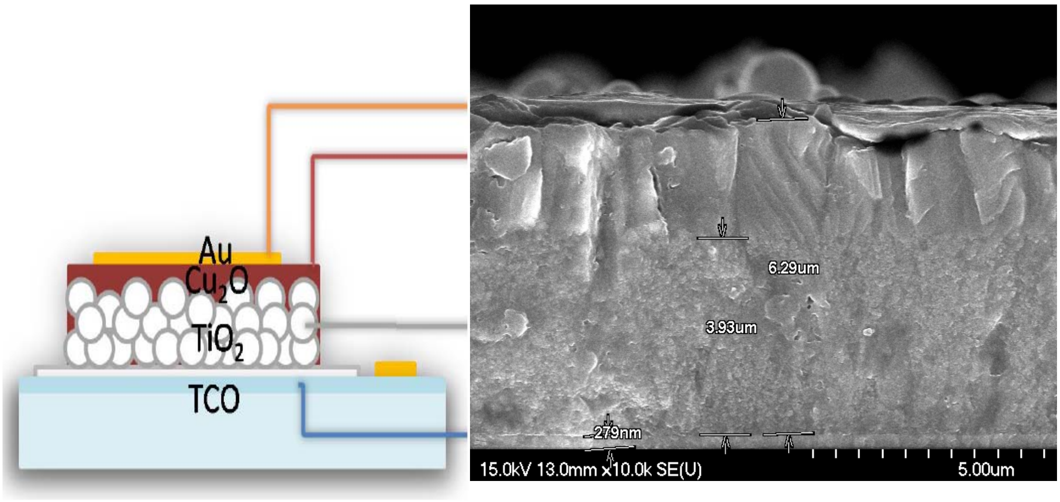

Fig.4.2 The complete Au/Cu_2O/TiO_2/TCO junction structure for measurement and the SEM cross-sectional image with indicated corresponding layers.

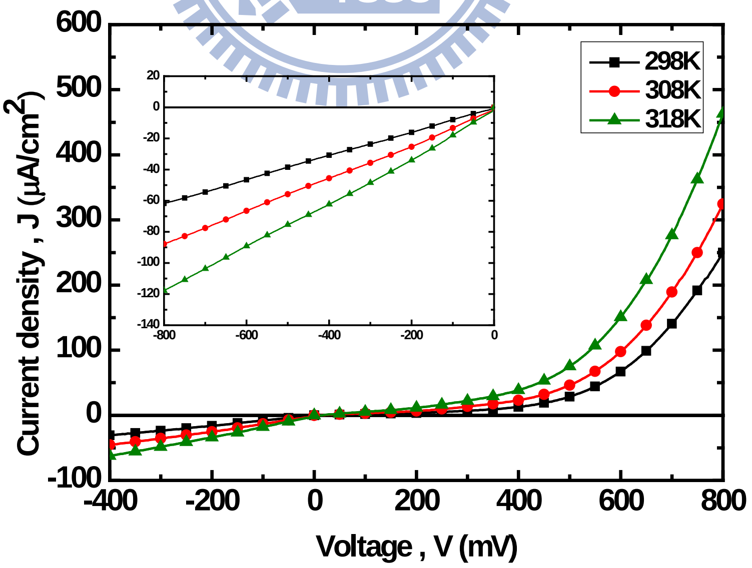

Fig.4.3 Forward and reverse current-voltage characteristics of the typically fabricated junction: Cu_2O 300μA/cm^2 4hr, P25 TiO_2 1.5μm, 20nm sputtered TiO_2 at elevated temperatures. Inserted picture is the enlarged reverse part.

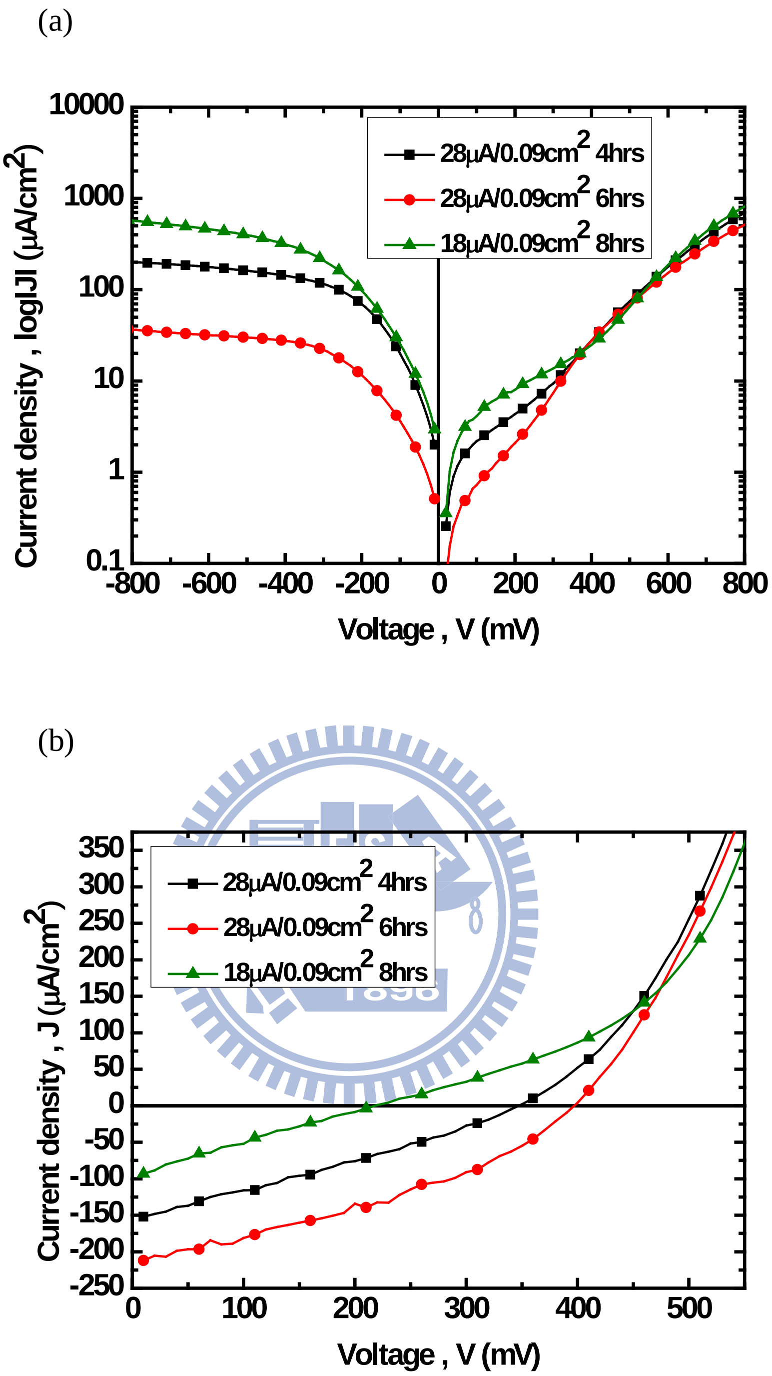

Fig.4.4 (a) Forward and reverse current-voltage characteristics in log scale of junctions and (b) 1sun illuminated current-voltage characteristics of junctions with three different Cu_2O depositing conditions:(1) 28μA/0.09cm^2 4hrs, (2) 28μA/0.09cm^2 hrs, and (3) 18μA/0.09cm^2 8hrs. All bottom layers were P25 TiO_2 1.5μm, 20nm sputtered TiO_2.

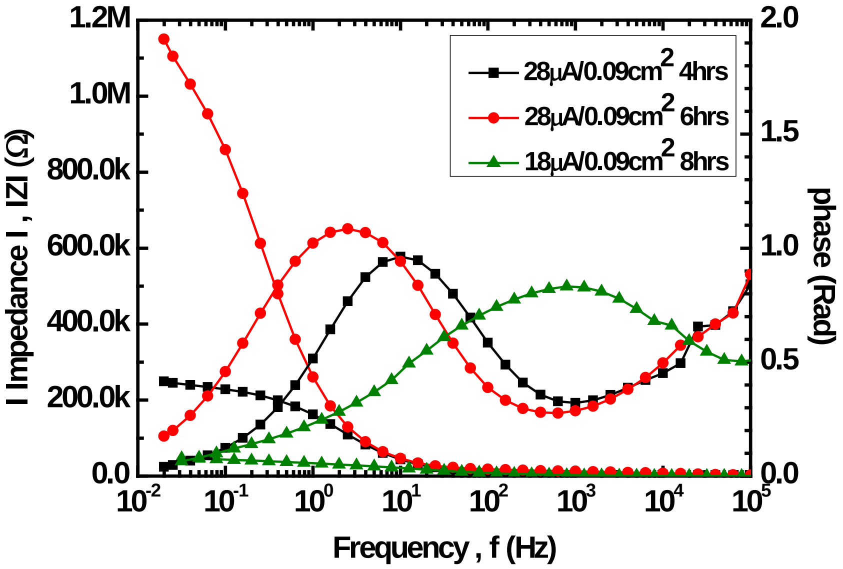

Fig.4.5 Impedance results of junctions with three different Cu_2O depositing conditions: (1) 28μA/0.09cm^2 4hrs, (2) 28μA/0.09cm^2 6hrs, and (3) 18μA/0.09cm^2 8hrs All bottom layers were P25 TiO_2 1.5 μm, 20nm sputtered TiO_2. All the samples were measured at zero bias, and the recorded frequency was ranged from 100kHz to 1mHz.

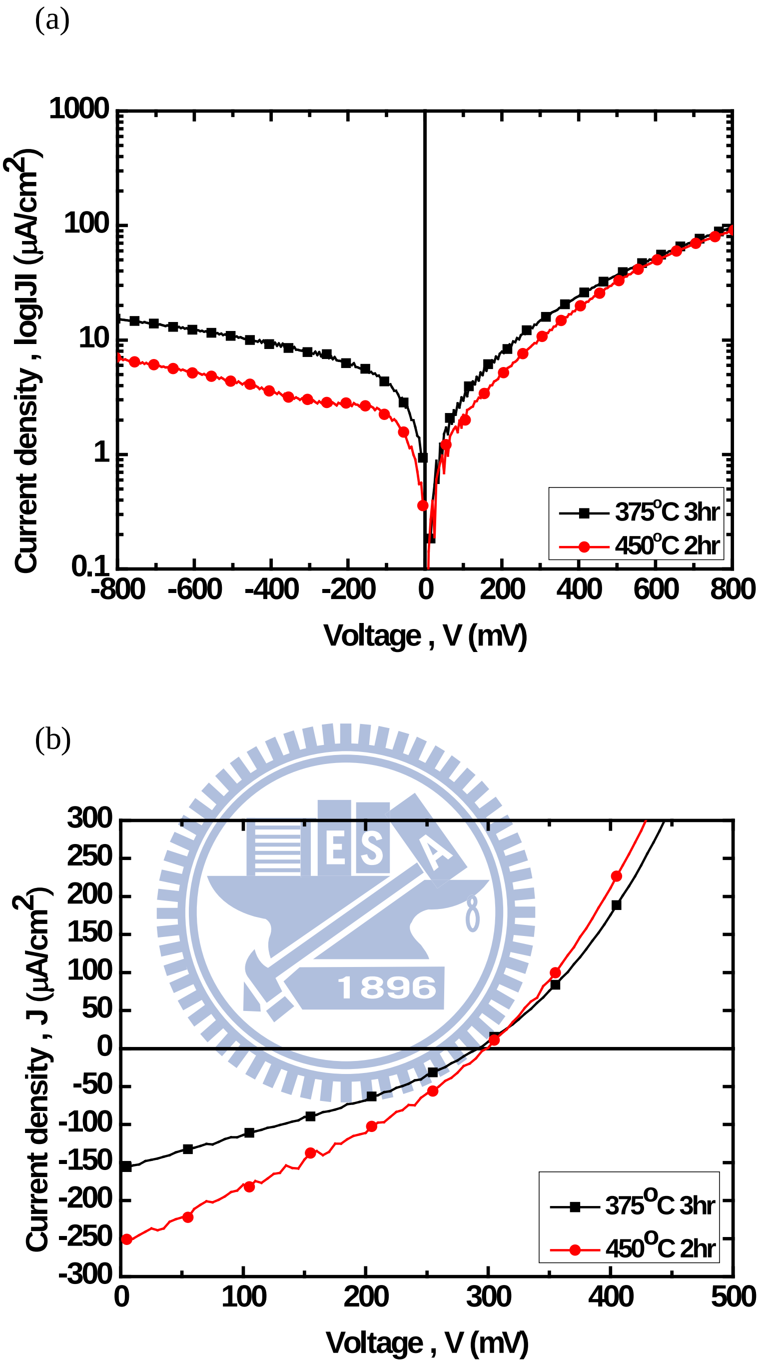

Fig.4.6 (a) Dark current and (b) photocurrent to voltage characteristics of junction with different annealing temperatures of TiO_2 : (1) 375℃ 3 hours (b) 450℃ 2 hours.

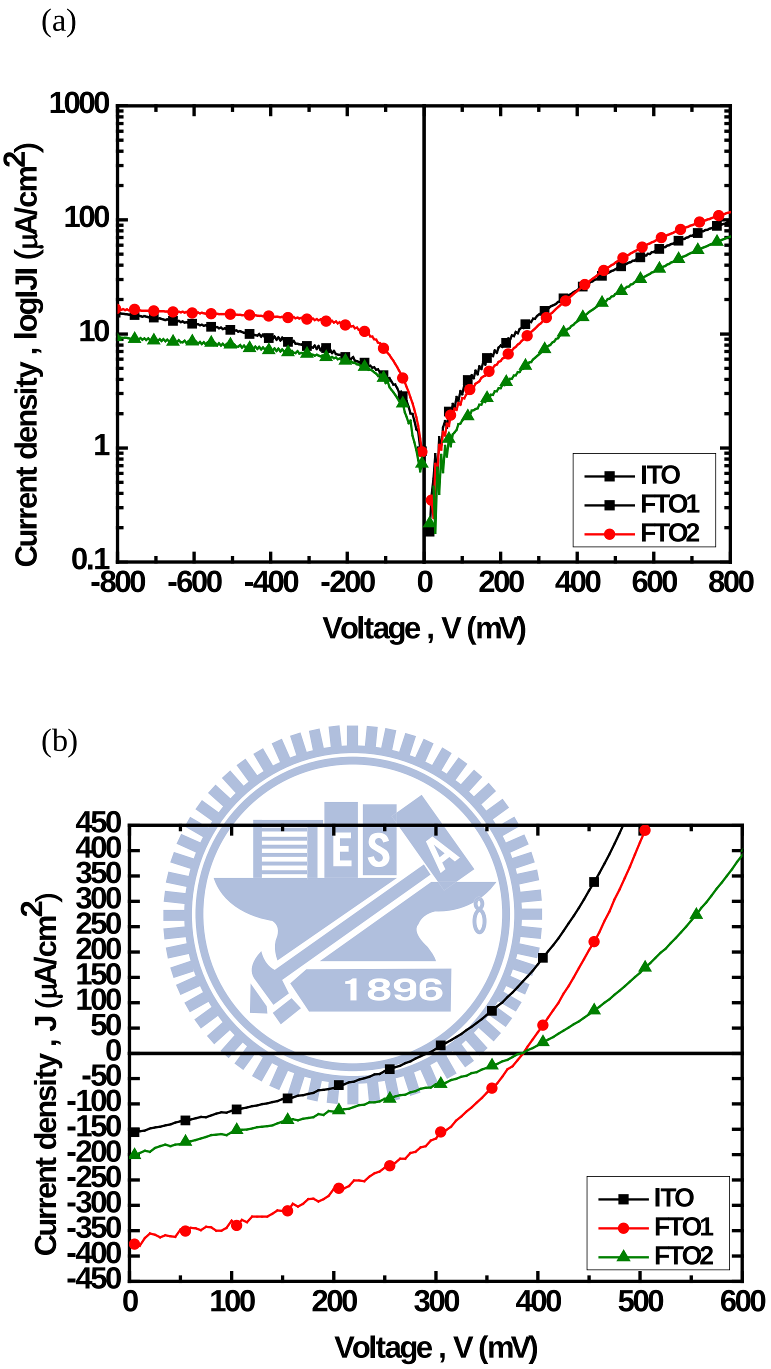

Fig.4.7 (a) Dark current and (b) photocurrent to voltage characteristics of junctions fabricated on different substrates:

(1) ITO: 20 Ω/□, (2) FTO1: 10 Ω/□, and (3) FTO2: 30 Ω/□

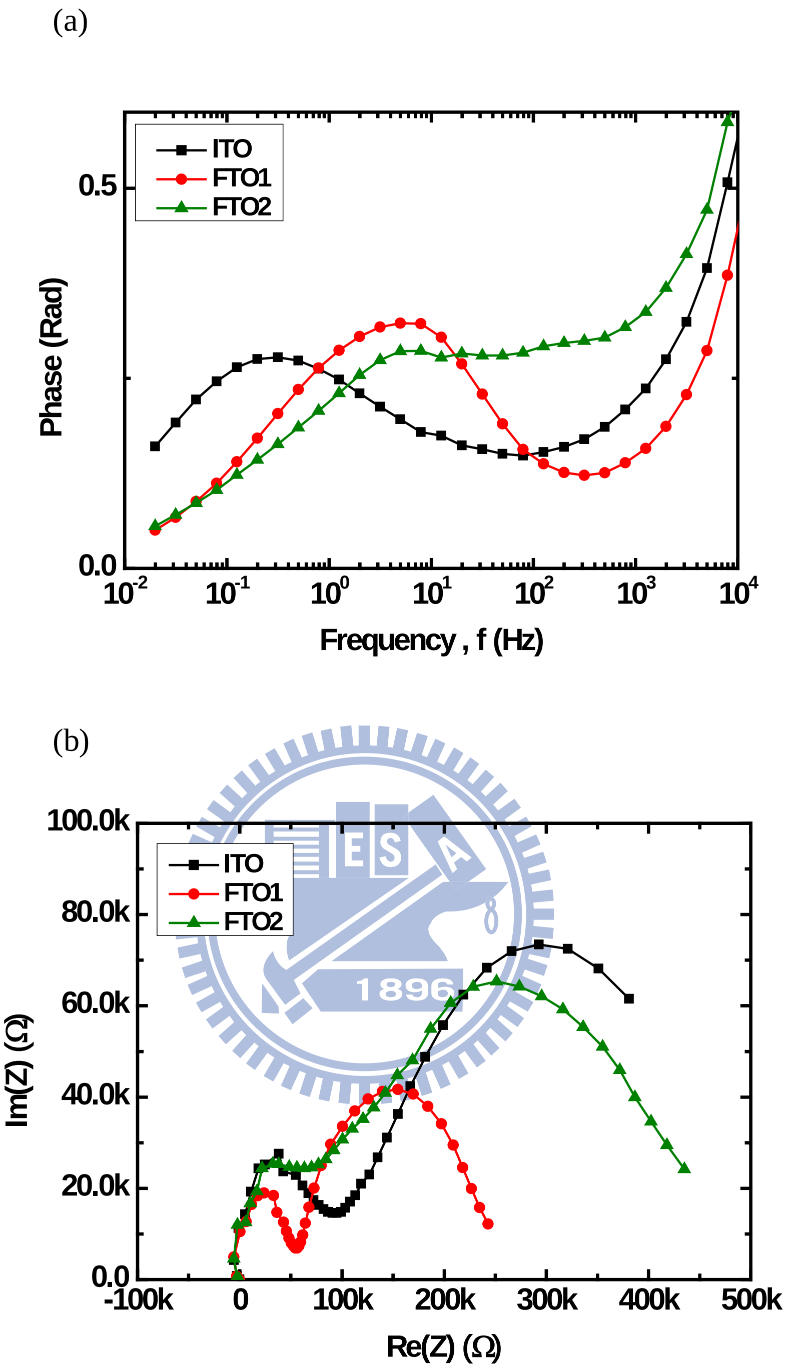

Fig.4.8 (a) EIS phase and (b) Nyquist plot of junctions fabricated on different substrates: (1) ITO: 20/□ (2) FTO1: 10 Ω/□ (3) FTO2: 30 Ω/□.

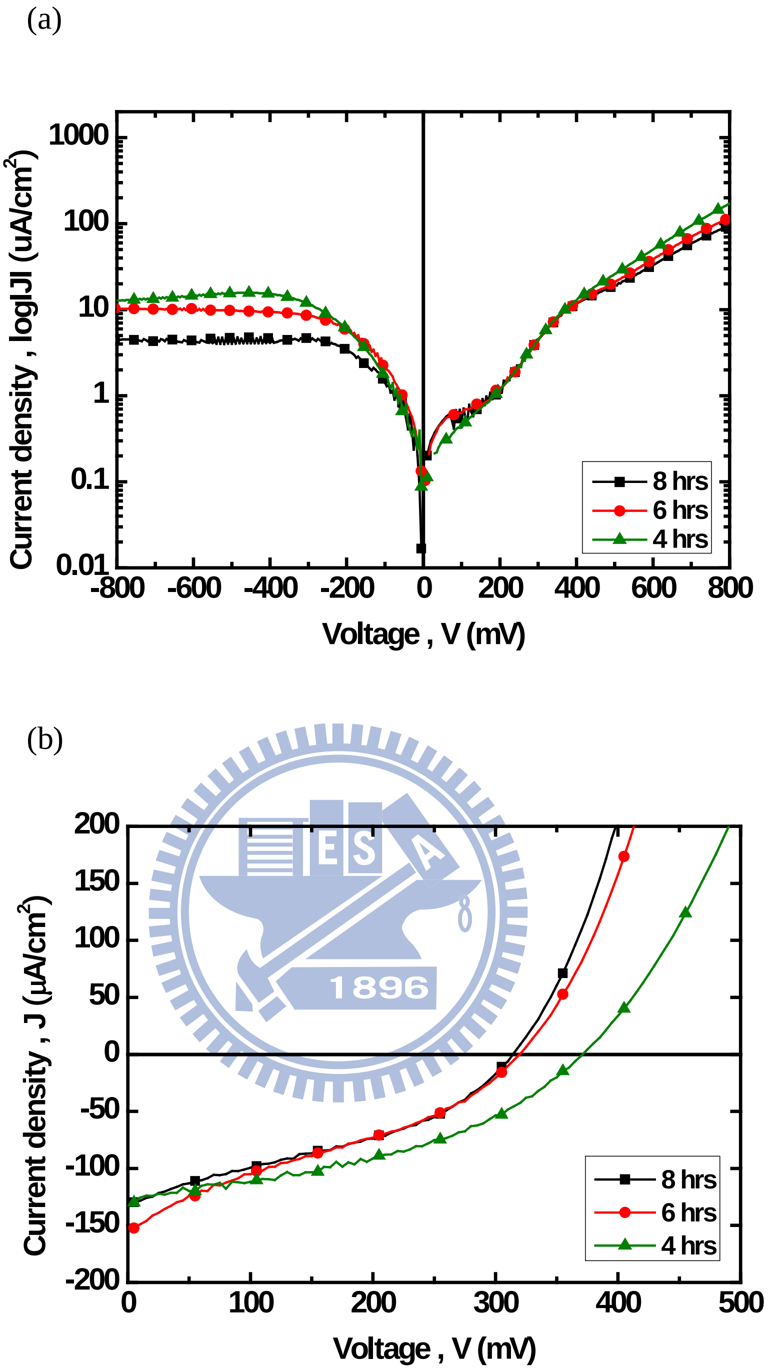

Fig.4.9 (a) Dark current and (b) photocurrent to voltage characteristics of junctions with different Cu_2O deposition time of (1) 3 hours, (2) 4 hours, and (3) 6 hours.

(a)

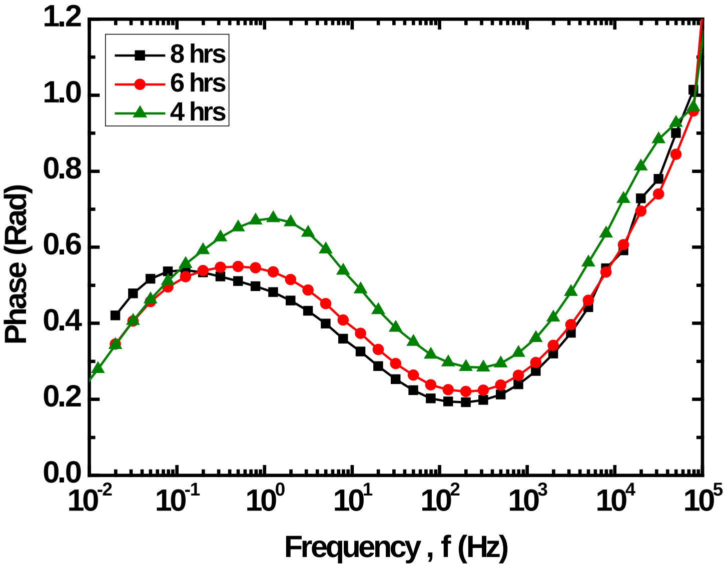

(b)

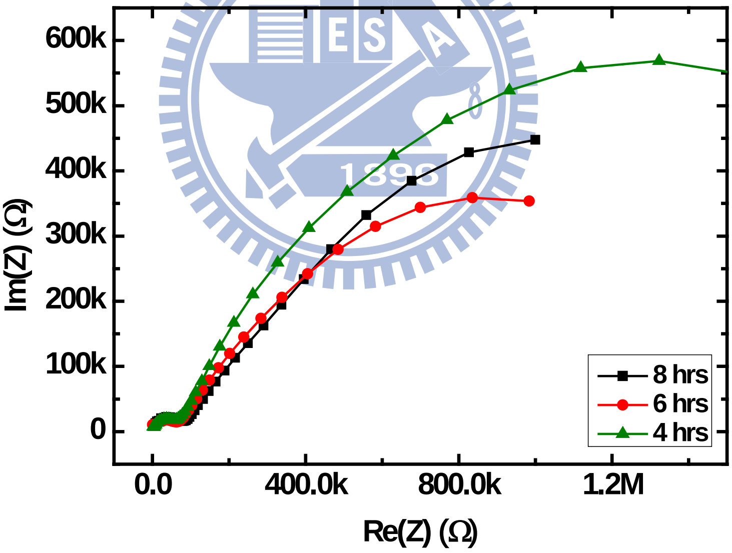

Fig.4.10 (a) EIS phase and (b) Nyquist plot of junctions with different Cu_2O deposition time of (1) 4 hours, (2) 6 hours, and (3) 8 hours.

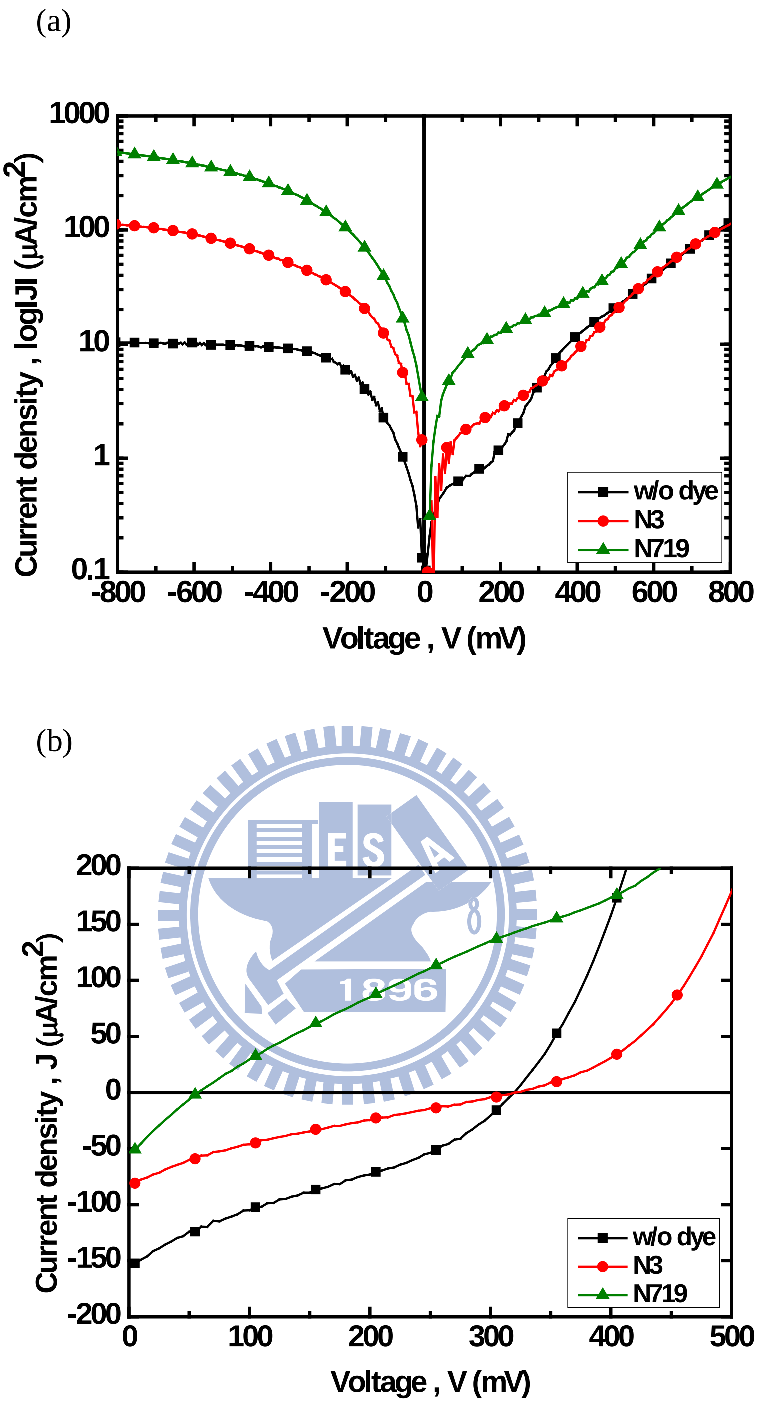

Fig.4.11 (a) Dark current and (b) photocurrent to voltage characteristics of junctions with or without dye absorption: (1) without dye absorption, (2) with N3 dye absorption, and (3) with N719 dye absorption.

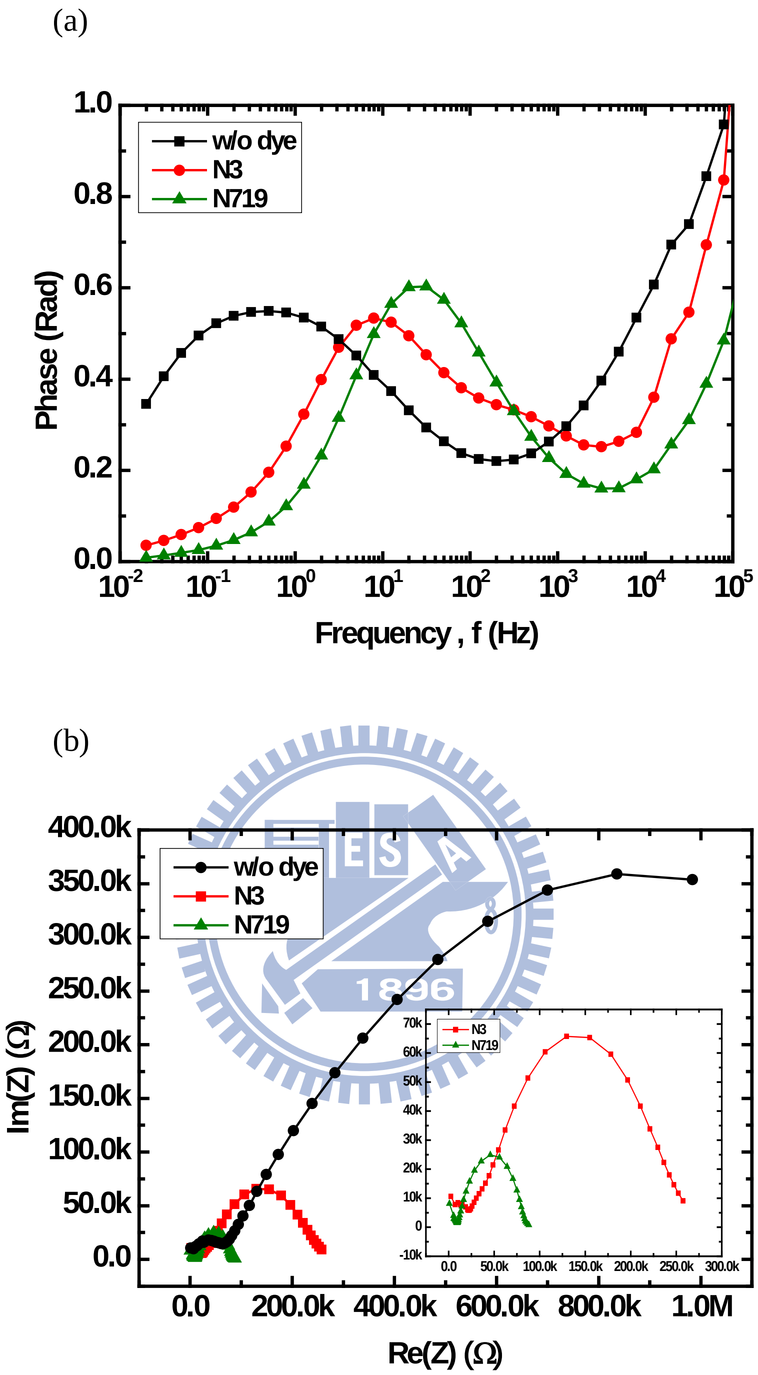

Fig.4.12 (a) EIS plot and (b) Nyquist plot of junctions with or without dye absorption: (1) without dye absorption, (2) with N3 dye absorption, and (3) with N719 dye absorption.

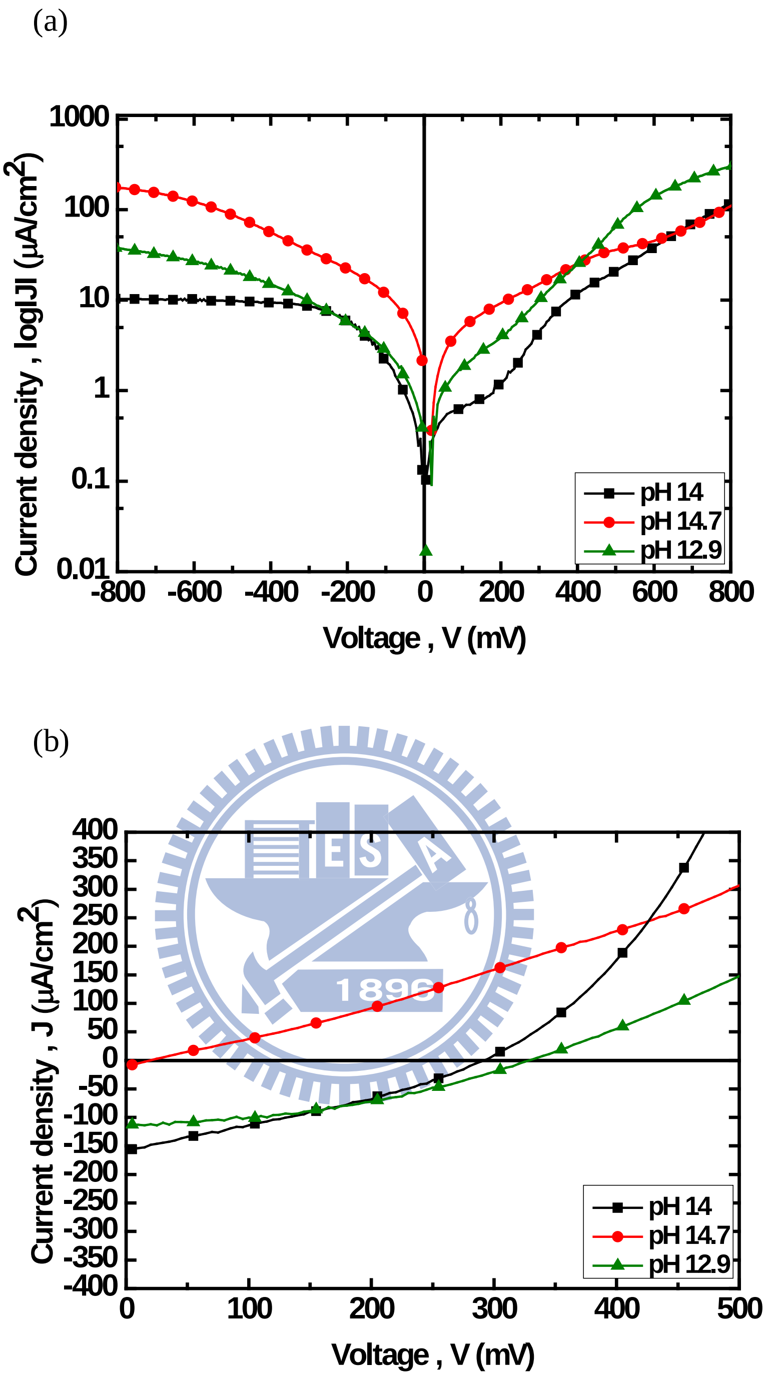

Fig.4.13 (a) Dark current and (b) photocurrent to voltage characteristics of junctions fabricated with different bath solutions of (1) pH 14.7, (2) pH 14, and (3) pH 12.

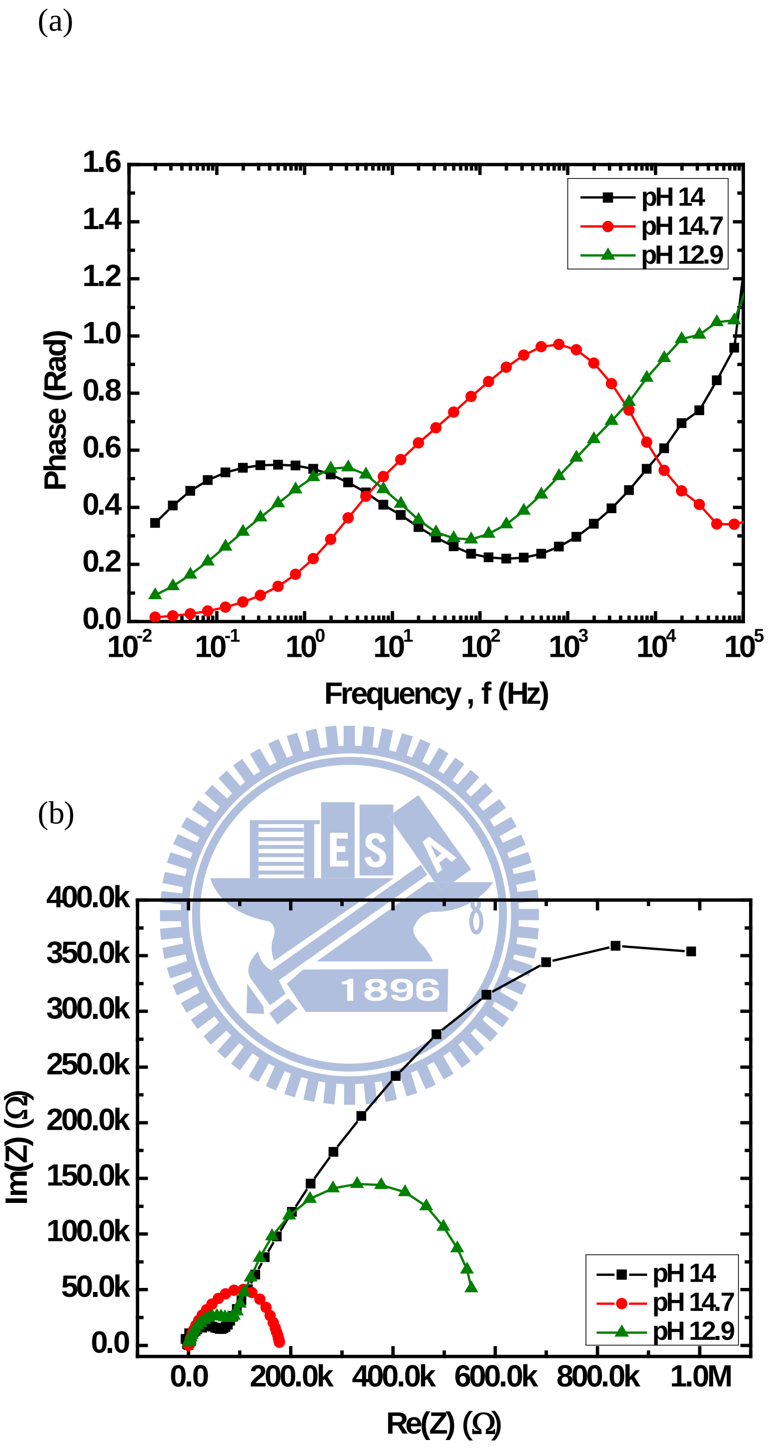

Fig.4.14 (a) EIS phase and (b) Nyquist plot of junctions fabricated with different bath solutions of (1) pH 14.7, (2) pH 14, and (3) pH 12.

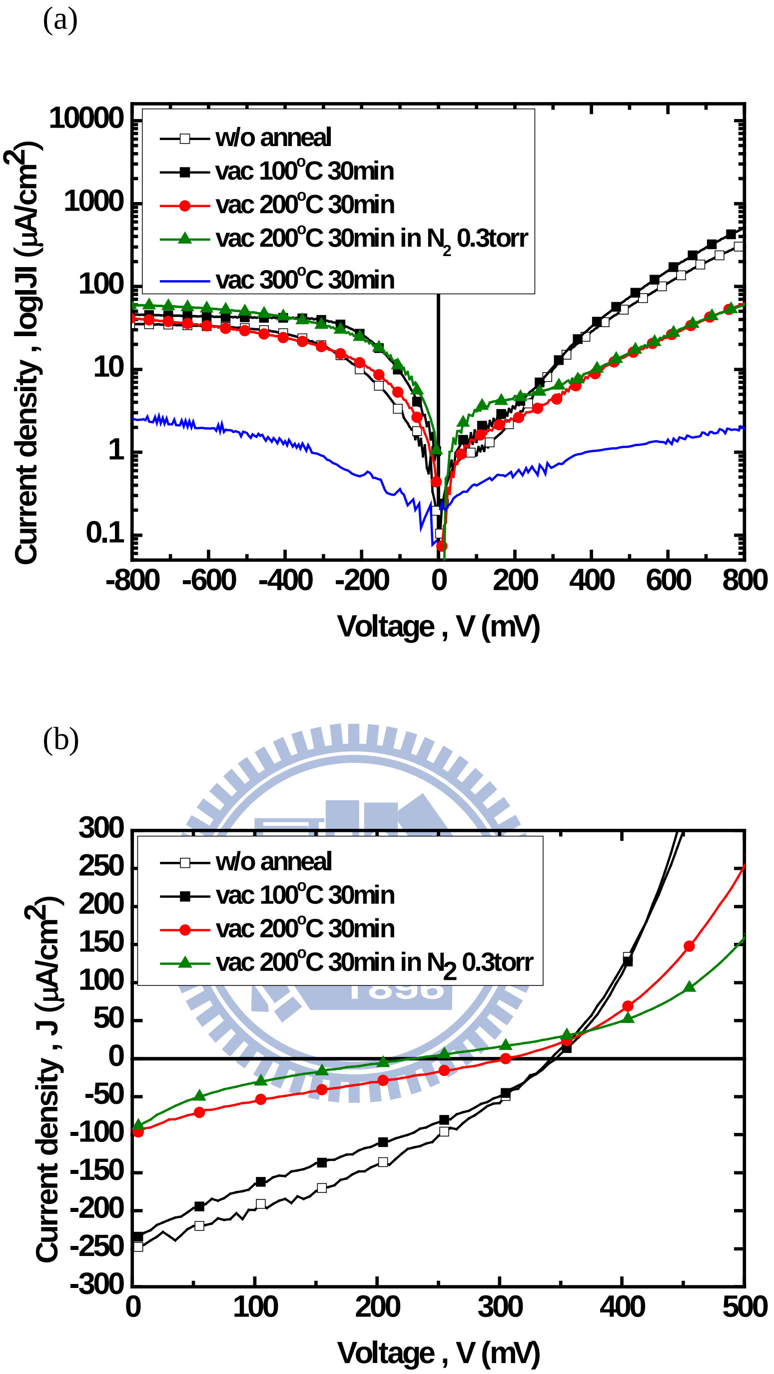

Fig.4.15 (a) Dark current and (b) photocurrent to voltage characteristics of junctions with different vacuum annealing temperatures of (1) 100℃, (2) 200℃, and (3) 300℃ for 30 minutes.

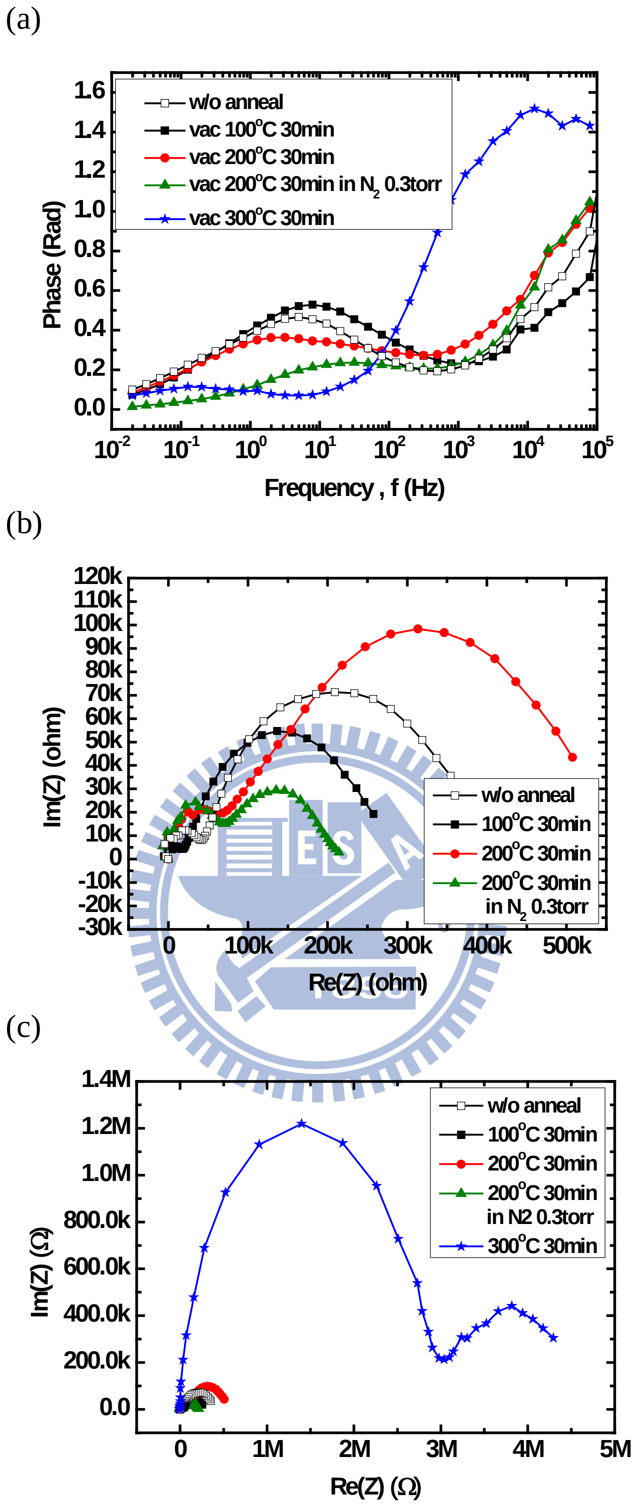

Fig.4.16 (a) EIS phase, (b) Nyquist plot, and (c) Nyquist plot of junctions with different vacuum annealing temperatures of (1) 100℃ (2) 200℃ (3) 300℃ for 30 minutes.

Chapter 5

Advanced Measurements

In the chapter four, the basic characteristics of the Cu_2O/TiO_2 bulk hetero-junction were examined. It was found that the suppression of recombination currents is a critical issue for applying the junction to DSSC. Only with sufficiently small recombination currents can we get better performance. Although many factors were considered and junctions were examined by the DC IV and AC EIS measurements, some advanced measurements were still needed to further understanding the characteristics of junctions. In this chapter, advanced measurements were conducted to investigate the temperature dependence, optical conditions, and voltage response of the Cu_2O/TiO_2 bulk hetero-junction. It is believed that with these thorough analyses, it will be helpful for our future researches.

5.1 Temperature dependence

In previously proposed paper [44], temperature dependent impedance result of DSSC was analyzed. Here, the temperature dependent IV and EIS measurements were both done to examine the effect of temperature to the characteristics of junction. Fig.5.1 shows the forward and reverse current to voltage characteristics of junctions with elevated temperatures from 298K to 338K, and both forward and reverse currents increased when the measuring temperature was elevated as the conventional p-n junction did. Besides, according to the temperature dependent equation of p-n junction forward current in the empirical form: $J_F \cong J_0 \exp(qV/kT) \propto \exp[-(E_g - qV)/kT]$, it is apparent that the forward current will increase approximately as $\exp[-(E_g - qV)/kT]$. In order to investigate the temperature dependence of junction current, current density to reciprocal temperature characteristics of junctions was examined, as shown in Fig.5.2 (a) and (b). It was obvious that the trend of curve was similar to the conventional p-n junction equation. Noted that we want to evaluate parameters from the current equation of conventional p-n junction, but owing to the bulk hetero-junction structure, which is dissimilar to conventional p-n junction, it is impossible for us to evaluate the parameters according to the current equation.

The EIS phase and Nyquist plot of junctions with elevated temperatures are shown in Fig.5.3 (a) and (b). The value of peak frequency, which is related to the recombination mechanism, shifted to higher value since the recombination current was increased with elevated temperature. Besides, the impedance value of circles in Nyquist plot, which is related to the resistance of the recombination currents, was also increased; and the trend of increased impedance values in Nyquist plot is the same as the elevated peak frequency values in phase plot.

5.2 Illumination intensity dependence

In the second part of the section, the light intensity dependence of junctions will be discussed. In this experiment, neutral density (ND) filters were used to modify the light intensity, and the light intensity will decay to 10^{-d} after pass through the ND filter, where d is the optical density. Table 5.1 shows the ND filters we used and its transmittances with relative neutral density. Fig.5.4 is the corresponding I-V characteristics under varied illumination intensities. The change in the photocurrent was apparent once the light intensity was modified; and the change in photo-voltage could also be identified, too. Besides, the current behavior in positive current region was due to the different optical conductance of junctions under different illumination intensities.

With larger light intensity, the larger excess charge will contribute to the larger optical conductance.

EIS result of junctions under different illumination intensities are examined as Fig.5.5 (a) and (b). From the phase plot, the variation of frequencies can be more accurately indentified. The result shows that the peak frequency values shifted to higher value with the increased light intensities except for the conditions of ND30 and ND20. There was little improvement of peak frequency when junction under weak light intensities. Besides, the trend of frequency shift in high frequency region was not the same as in middle frequency region; therefore, the electron behavior in high frequency region was not caused by recombination mechanism. In Nyquist plot, the trend of impedance value change also corresponded to the EIS phase result; and both high frequency circle and middle frequency circle were affected by the modified light intensities. There was a large deviation of the impedance values for junctions under illumination condition compared to junctions under dark condition.

Optical response was also examined for junctions with different Cu_2O deposition time to investigate whether the Cu_2O thickness could affect the optical response. Fig.5.6 (a), (b) and (c) show the results of junctions under different illumination intensities with Cu_2O deposition time of 8 hours, 6 hours, and 4 hours, respectively. It seemed that there was no apparent divergence of these junctions under different light intensities; and the change of photocurrent and photo-voltage with the change of illumination intensities was also identified as before.

5.3 Voltage response – Mott-Schottky (M-S)

Mott-Schottky analysis [45-47] is an useful technique to examine the characteristics of thin films and junctions. It can provide us information about the flat-band potential and carrier concentration in devices by examined its related capacitance response to voltage under appropriate frequency range. The flat-band potential of TiO_2 electrode and CuSCN film was obtained in the previously proposed paper [48], and the correlate energy band model was constructed with the Mott-Schottky results. The flat-band potential can be obtained according to the M-S equation: $\frac{1}{C^2} = \frac{2}{\varepsilon\varepsilon_o e N_A A^2}\left(-V_0 + V_{fb} - \frac{kT}{e}\right)$, where C is the space-charge capacitance, ε is the dielectric constant of Cu_2O, ε_o is the permittivity of free space, N_A in the density of acceptors in Cu_2O, A is the electrode area, V is the bias potential, k is the Boltzmann constant, T is the absolute temperature and e is the electronic charge; and by extrapolating the linear part to the potential axis in the C^{-2} vs V plot, the flat-band potential can be obtained.

In the final part of the thesis, EIS measurement was conducted under positive and negative bias to investigate the voltage response of the junction. With the extraction of the EIS data, we try to acquire the information about the variation of capacitance with different voltage bias and obtain the Mott-Schottky result. Fig.5.7 (a) and (b) shows the phase and Nyquist plot of junctions under positive voltages from 0V to +0.6V, it is obvious that the trends of peak frequency shift in EIS phase and impedance circle change in Nyquist plot were similar. Base on the results investigated, it seems that there were some similar characteristics of junctions under forward bias in dark condition and under illumination conditions; and further researches were needed to explain the characteristics. Fig.5.7 (c) is the Mott-Schottly plot extracted from the EIS results. With linear fitting in the negative bias part, flat-band potential of -0.23V was acquired; but the acquired flat-band potential value is not correct since it must be a positive value. The deviation of flat-band potential is due to incorrect frequency region of extracted EIS results. The Mott-Schottky plot is acquired by extracting the circle related to the middle frequency region, which corresponded to recombination mechanism but not the junction capacitance.

Fig.5.8 (a) is the EIS phase of junction under 0.2V bias, the high frequency region of phase plot was not complete since the limitation of our equipment, which the highest frequency value is about 1M Hz. So frequency response of junctions beyond 1M Hz cannot be measured, and the response measured near limited frequency value was not accurate. The equipment limitation restricts our research of frequency response. Fig.5.8 (b) shows the Nyquist plot of junctions under the same bias condition, the incomplete circle related to high frequency region is observed. It seemed that if we can extract the capacitance values from high frequency region, we may acquire the more correct flat-band potential value.

In an attempt to prove our guess, we extracted the capacitance values from the high frequency region in Nyquist plot, although the EIS result is not complete, and compared it to that extracted from middle frequency region. The Mott-Schottky results extracted from different frequency ranges are shown in Fig.5.9 (a) and (b). The flat-band potential in Mott-Schottky plot extracted from middle frequency is -0.207V, and the one extracted from high frequency region is -0.176V. Although it was still a negative value, the positive shift accorded to our speculation. Noted that the impedance magnitude near the high frequency region was not accurate, hence the Mott-Schottky result was not completely correct; but the trend of positive shift still existed. From the results we investigated, it is believed that with high frequency range, we can acquire more complete information from the EIS results. Therefore, we can obtain the more accurate Mott-Schottky plot and construct the energy band model.

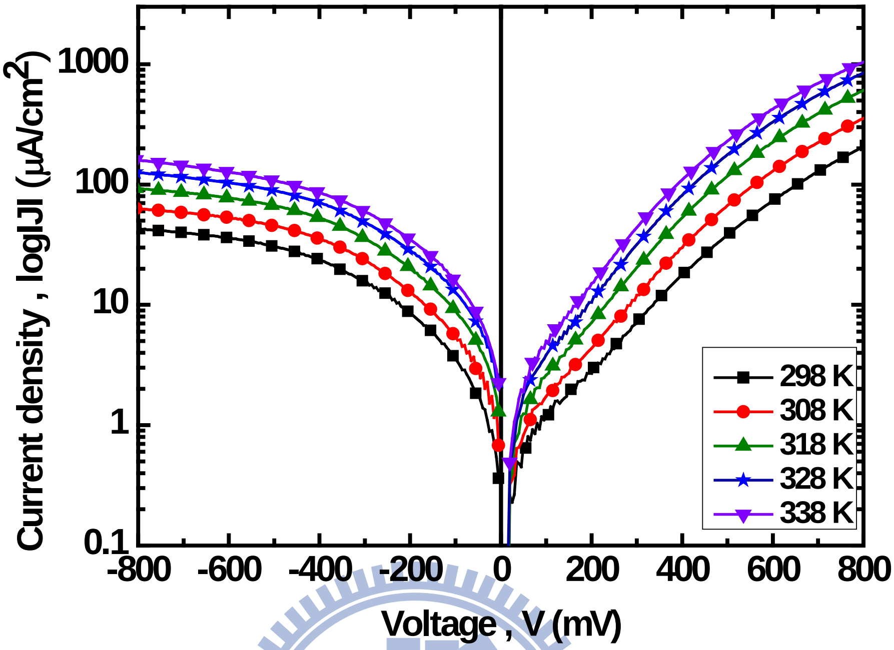

Fig.5.1 Forward and reverse current to voltage characteristics of junctions with elevated temperatures: (1) 298K, (2) 308K, (3) 318K, (4) 328K, and (3) 338K.

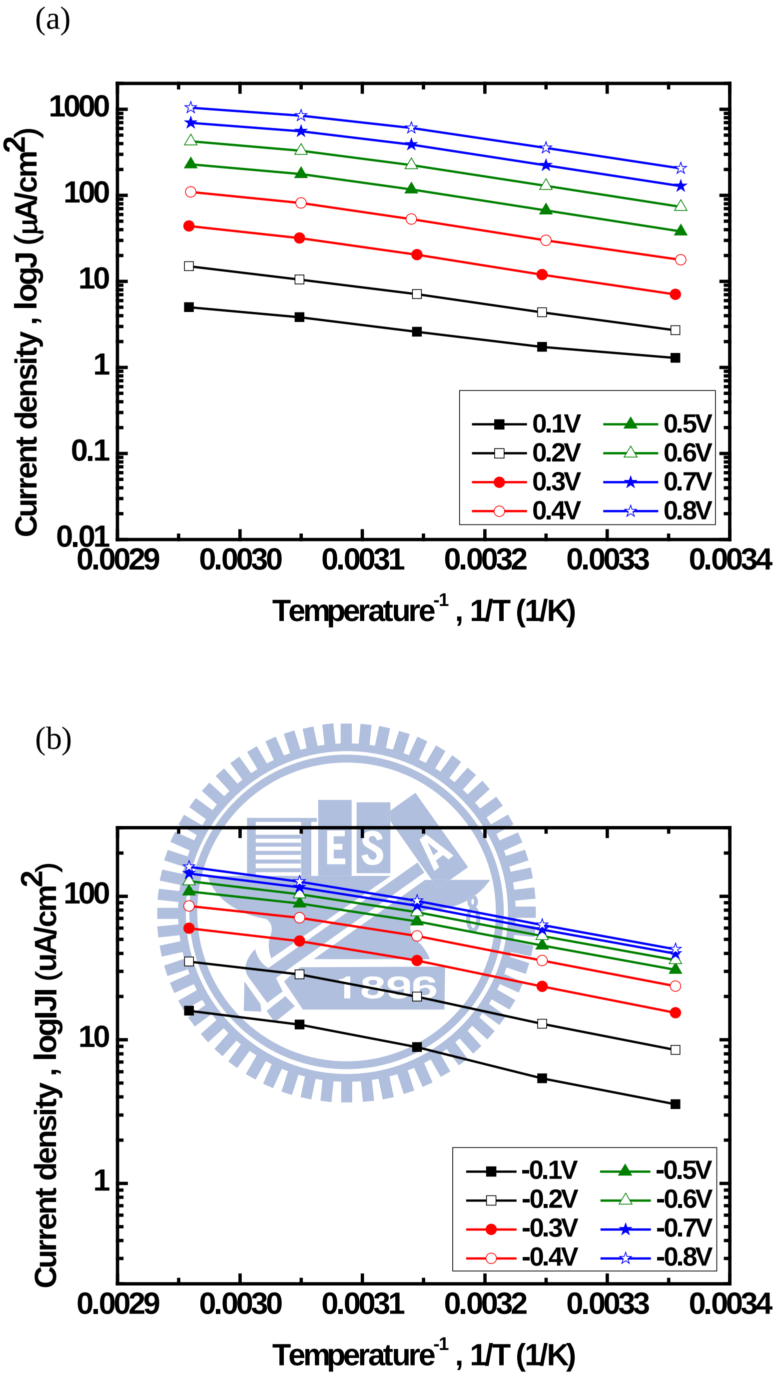

Fig.5.2 LogJ to reciprocal temperature plot of junctions in (a) forward bias, and (b) reverse bias region with elevated temperatures: (1) 298K, (2) 308K, (3) 318K, (4) 328K, and (3) 338K.

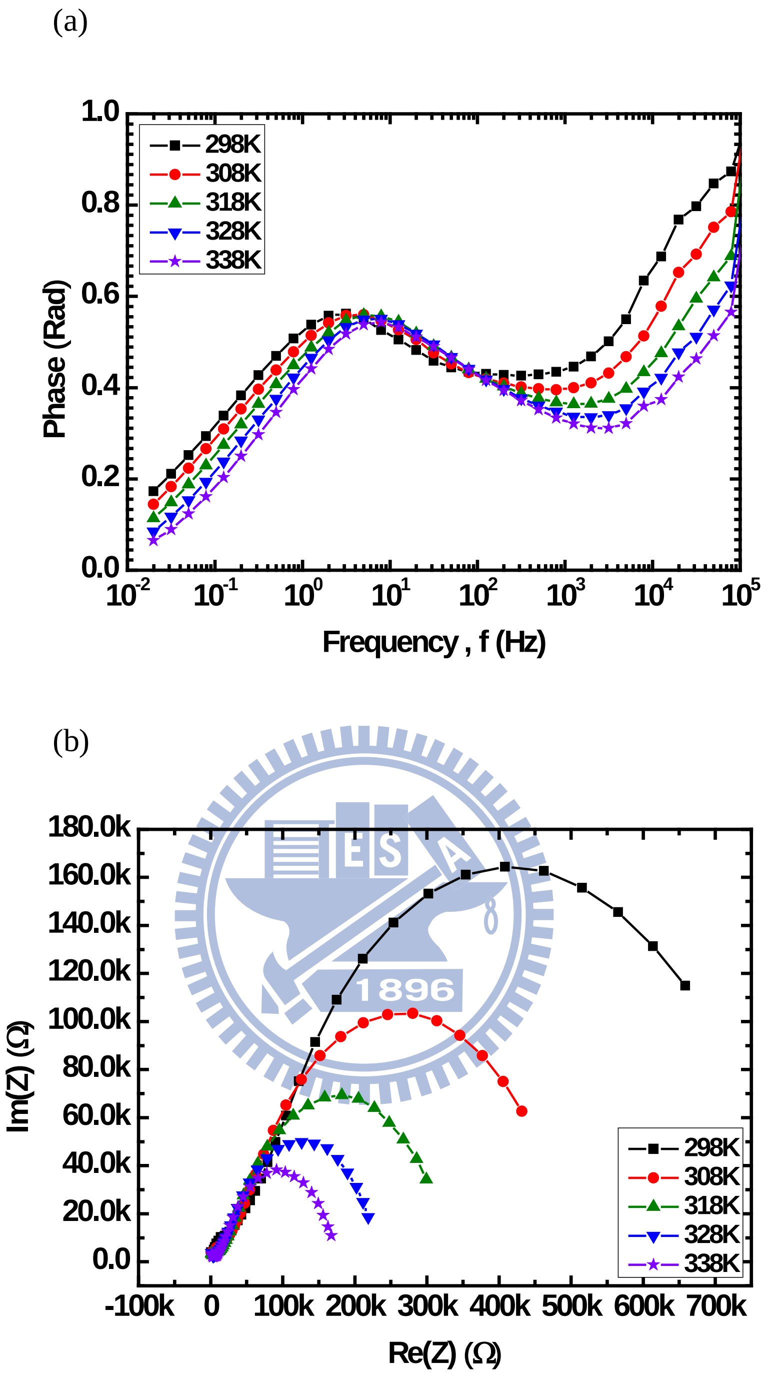

Fig.5.3 (a) EIS phase and (b) Nyquist plot of junctions with elevated temperatures: (1) 298K, (2) 308K, (3) 318K, (4) 328K, and (3) 338K.

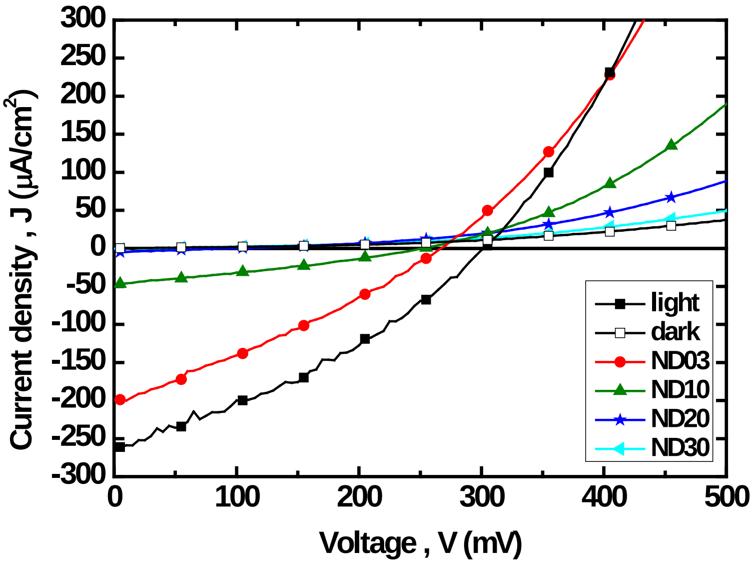

Fig.5.4 Photocurrent to voltage characteristics of junctions under varied illumination intensities.

Table 5.1

ND filter	d (optical density)	% transmittance
ND03	0.3	50 %
ND10	1.0	10 %
ND20	2.0	1 %
ND30	3.0	0.1 %

Table 5.1 The ND filters we used and its transmittances with relative neutral density.

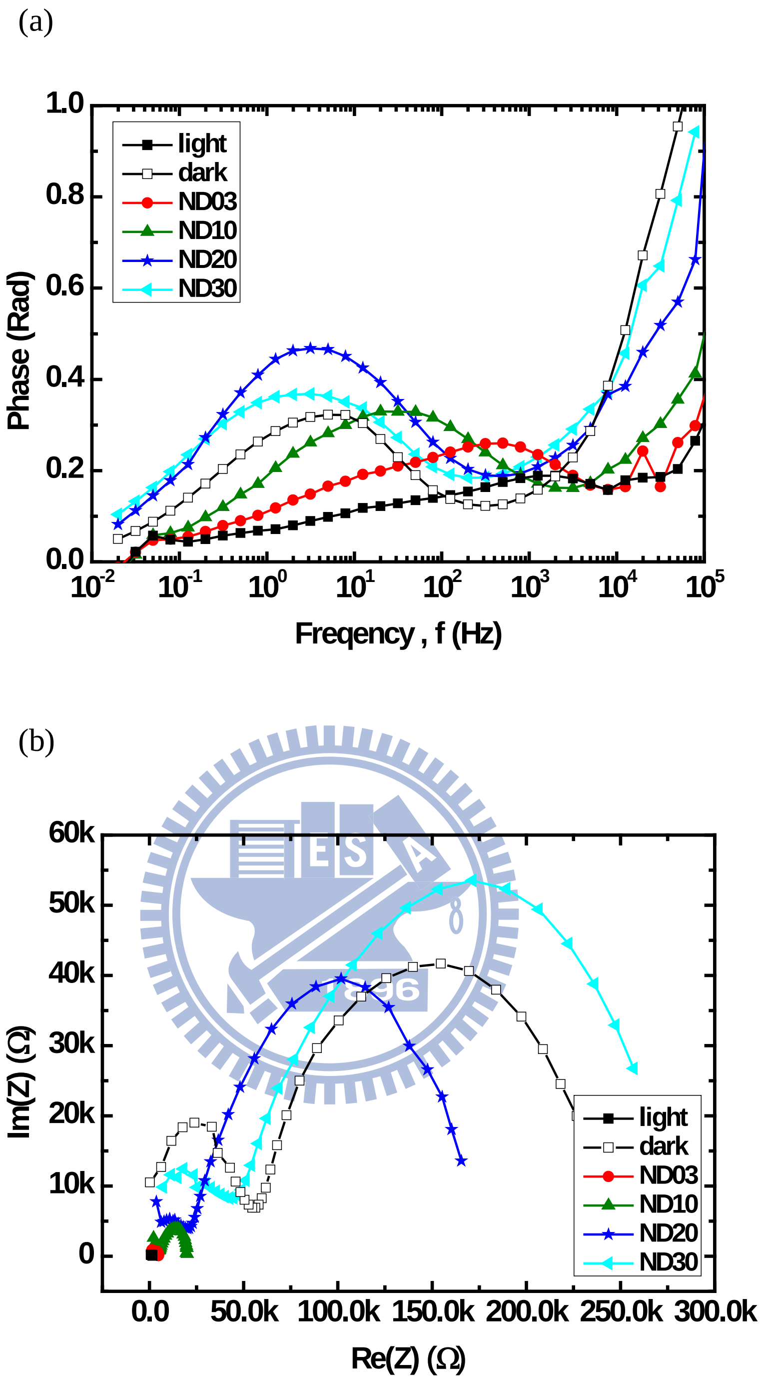

Fig.5.5 (a) EIS phase and (b) Nyquist plot of junctions under varied illumination intensities.

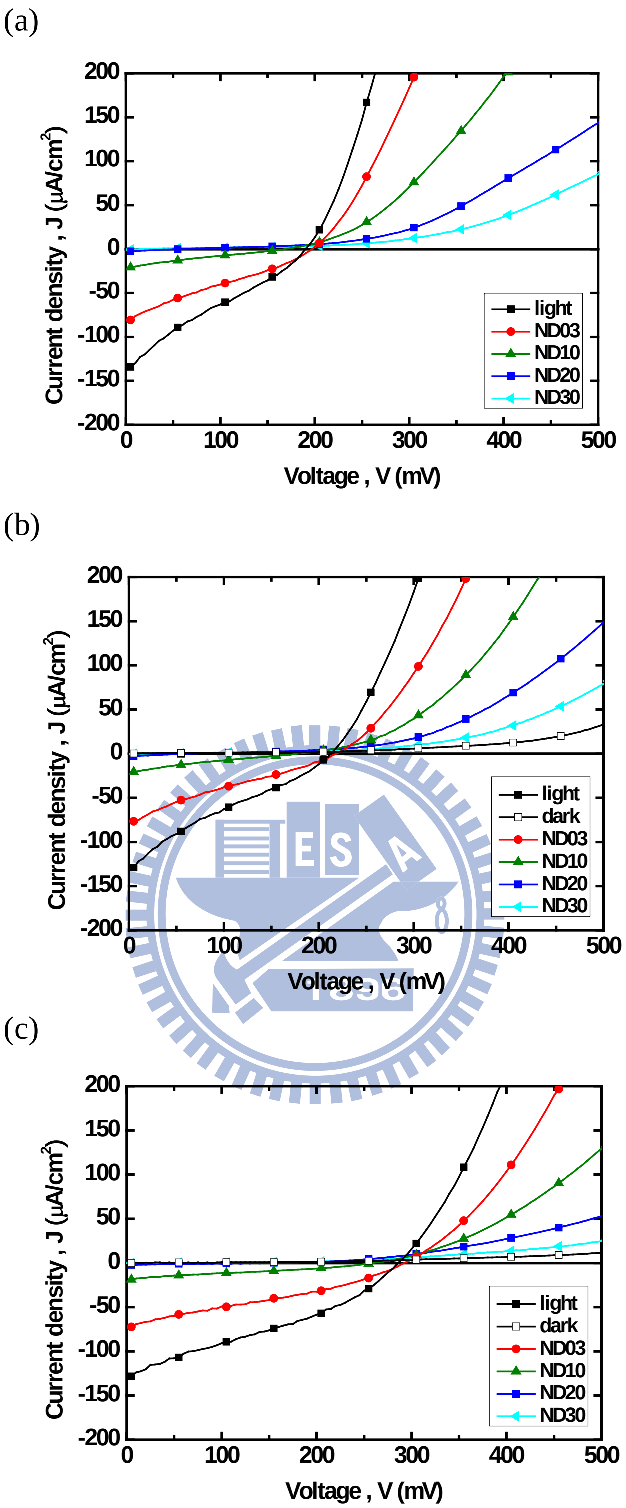

Fig.5.6 Photocurrent to voltage characteristics of junctions with different Cu_2O deposition time of (a) 8 hours, (b) 6 hours, and (c) 4 hours under varied illumination intensities.

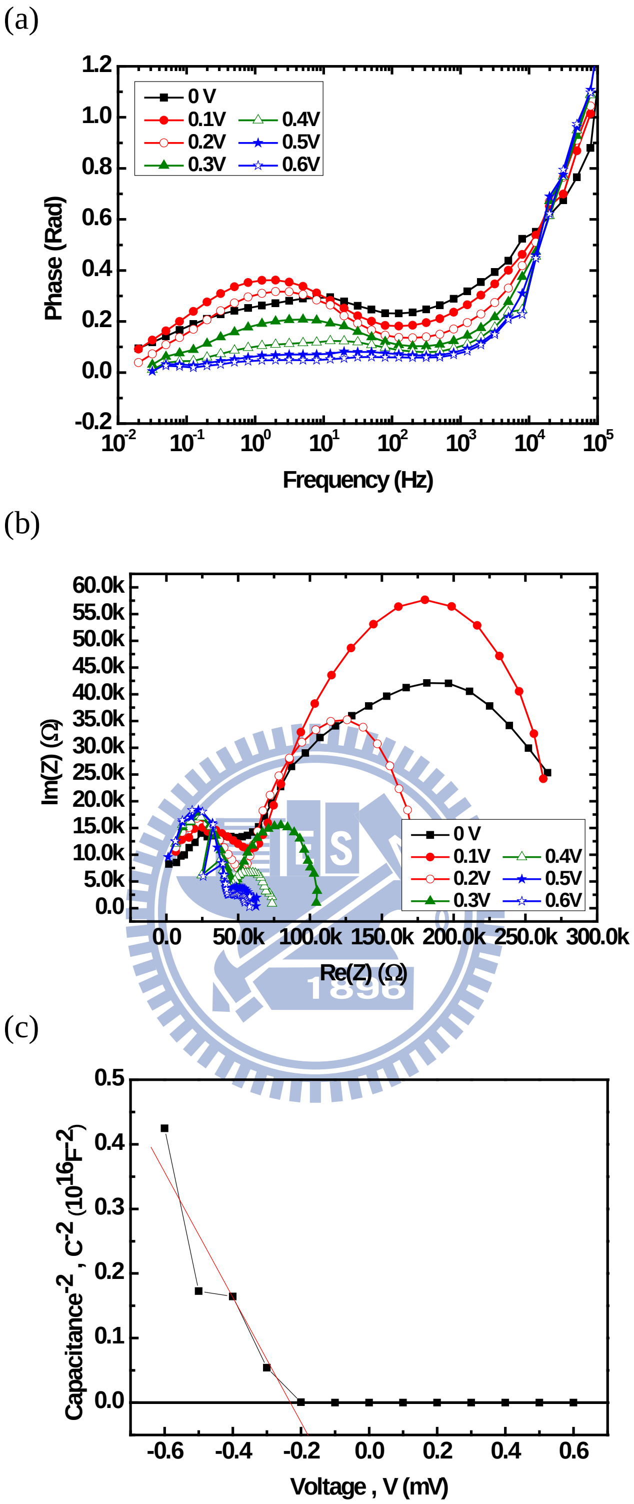

Fig.5.7 (a) EIS phase and (b) Nyquist plot of junctions with positive voltages from 0V to +0.6V, and (c) Mott-Schottky plot extracted from the EIS results.

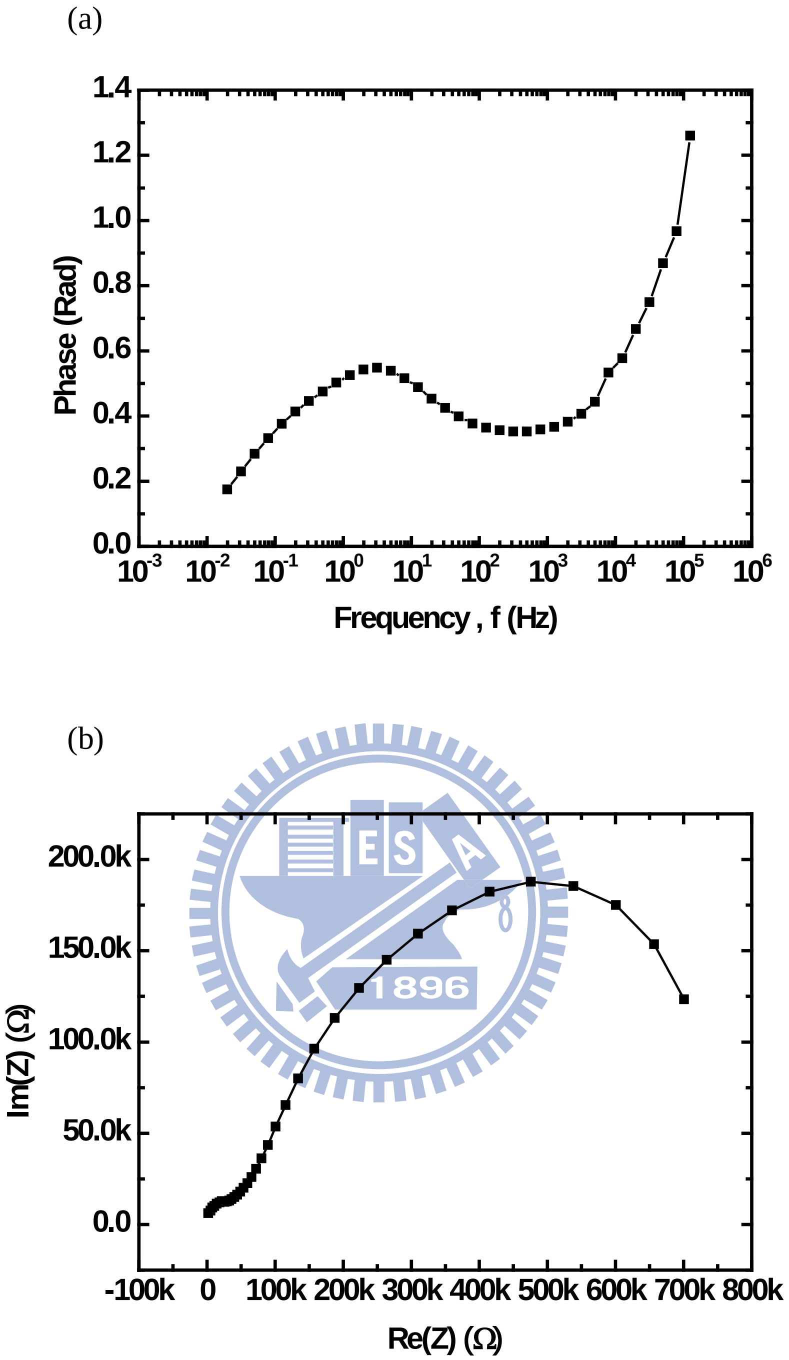

Fig.5.8 (a) EIS phase and (b) Nyquist plot of junctions under 0.2V bias.

(a)

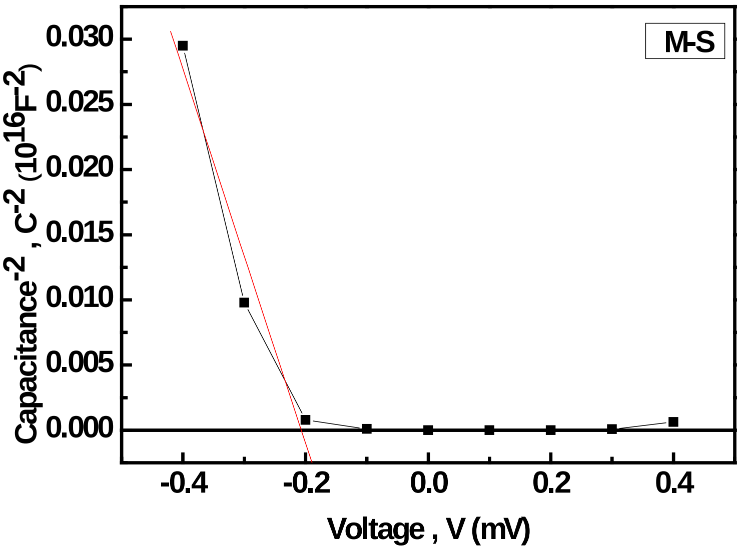

(b)

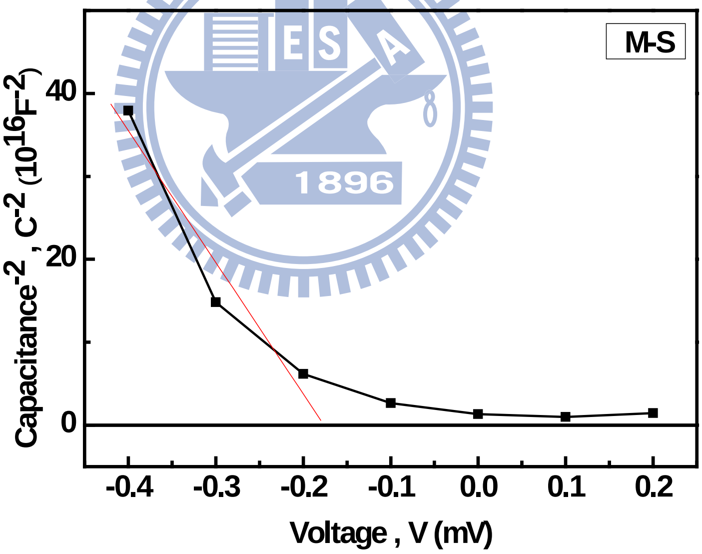

Fig.5.9 Mott-Schottky plot of junctions extracted from (a) middle frequency region, and (b) high frequency region.

Chapter 6

Summary and Outlook

Dye sensitized solar cell, fabricated with inexpensive methods and materials, is an attractive candidate for photovoltaic device. It has shorter payback time in comparison with conventional solar cells since the demand of the purity of materials used in DSSC is less. Although there are many advantages, the main problem of DSSC is the long time stability. Generally speaking, the degradation on the sealant is hard to avoid and will cause the leakage of electrolyte. In order to improve the drawback, it seems necessary to replace the electrolyte with solid-state materials. In this thesis, Cu_2O was adapted as a p-type material to replace the electrolyte layer and the basic characteristics of Cu_2O/TiO_2 bulk hetero-junction were investigated.

At the beginning of the experiment, two kinds of deposition methods of electrochemical deposition are examined, including galvanostatic method and potentialstatic method. After the choice of appropriate method, variety conditions of Cu_2O deposition are examined, such as bath pH value, and current density. Besides, the deposition condition is related to the surface properties of matter on which we deposited. With the analyses of XPS and XRD results, correct composition and best condition was found. By adapting the best deposition condition, a complete Cu_2O/TiO_2 bulk hetero-junction was formed successfully.

Next, the basic understanding of the junction is constructed by current to voltage measurement and electrical impedance spectroscopy measurement. There are many similar characteristics between the bulk hetero-junction and conventional p-n junction. Besides, it is found that inhibition of recombination centers of the junction is a critical issue to improve the optical performance. Therefore, many conditions are applied to the junctions and the characteristics of junctions are examined. With different conditions and the measurement results, we can advanced characterized the bulk hetero-junction.

Afterward, many advanced measurements are performed to help us to comprehend the temperature dependence, optical condition, and voltage response of the Cu_2O/TiO_2 bulk hetero-junction. Furthermore, the voltage response of the junction can let us acquire the Mott-Schottky plot to calculate the flat-band potential and carrier concentration and even construct the energy band model. Unfortunately, the frequency range of EIS measurement we used is not higher enough now to measure the higher frequency response, which is related to the junction itself, of the junction.

In conclusion, the Cu_2O/TiO_2 bulk hetero-junction is formed successfully by electrochemical deposition method in the first time. Before applying to DSSC, the recombination centers of junction should be eliminated first. Since the deposition condition is dependent on the TiO_2 surface, the conditions of Cu_2O deposition on dyed-TiO_2 surface may be different from now. As a result, further researches are needed to find the best condition of Cu_2O deposition on the dyed-TiO_2 surface. Additionally, Cu_2O film can also used in nano-tube structure DSSC, and apparently, the deposition condition must be different again since the surface properties of nano-tube structure is not the same as the nano-porous structure.

References

[1] V. Fthenakis; E. Alsema, *Progress in Photovoltaics*, 2006, 14, 3, 275.

[2] M.J. de Wild-Scholten; A.C. Veltkamp, *Environmental Life Cycle Analysis of Dye Sensitized Solar Devices; Status and Outlook; ECN Solar Energy.*

[3] B. O'Reagen; M. Grätzel, *Nature* 1991, 353, 6346.

[4] Michael Grätzel, *Journal of Photochemistry and Photobiology A: Chemistry* 164 (2004) 3–14

[5] Papageorgiou, N.; Athanassov, Y.; Armand, M.; Bonhote, P.; Pettersson, H.; Azam,A.; Grätzel, M. *J., Electrochem. Soc.* 1996, *143*, 3099.

[6] Murakoshi, K.; Kogure, R.; Wada, Y.; Yanagida, S., *Sol. Energy Mater. Sol. Cells* 1998, *55*, 113.

[7] Yanagida, S.; Kambe, S.; Kubo, W.; Murakoshi, K.; Wada, Y.; Kitamura, T. *Z., Phys. Chem. Part 1* 1999, *212*, 31-38.

[8] K Tennakone, G R R A Kumara, A R Kumarasinghe, K G U Wijayantha and P M Sirimanne, *Semicond. Sd. Technol.* 10 (1995) 1689-1693.

[9] B. O'Regan; F. Lenzmann; R. Muis, J. Wienke, *Chem. Mater.* 2002, 14, 5023.

[10] G.R.R.A. Kumaraa, A. Konnoa, G.K.R. Senadeerab, P.V.V. Jayaweerab, D.B.R.A. De Silvab, K. Tennakone, *Solar Energy Materials & Solar Cells* 69 (2001) 195–199

[11] Taketo Taguchi; Xin-tong Zhang; Irwan Sutanto; Ken-ichi Tokuhiro; Tata. N. Rao; Hiroko Watanabe; Toshie Nakamori; Masayuki Uragamic; Akira Fujishima, *Chem. Comm.* 2003, 19, 2480–2481.

[12] Peter Chen; Jun Ho Yum; Filippo De Angelis; Edoardo Mosconi; Simona Fantacci; Soo-Jin Moon; Robin Humphry Baker; Jaejung Ko; Md. K. Nazeeruddin; Michael Grätzel, *Nano Lett.*, 2009, 9 (6), 2487–2492.

[13] Qing Wang; Kai Zhu; Nathan R. Neale; Arthur J. Frank, *Nano Lett.*, 2009, 9 (2), pp 806–813

[14] B. O'Regan; D. T. Schwartz; S. M. Zakeeruddin; M. Grätzel, *Adv. Mater.* 2000, 12, No. 17, pp 1263-1267

[15] W.B. Wu; Z.G. Jin; G.D. Hu; S.J. Bu, *Electrochimica Acta* 52 (2007) 4804–4808

[16] C. Rost; I. Sieber; S. Siebentritt; M. C. Lux-Steiner; R. Könenkamp *APPLIED PHYSICS LETTERS*, 1999, Vol.75, No.5, pp 692–694

[17] Benjamin D. Yuhas; Peidong Yang, *J. AM. CHEM. SOC.* 2009, 131, 3756–3761

[18] N.R. de Tacconi, C.R. Chenthamarakshan, K. Rajeshwar, T. Pauporté, D. Lincot, *Electrochem. Commun.* 5 (2003) 220.

[19] S. Peulon and D. Lincot, *J. Electrochem. Soc.* 145 (1998), p. 864

[20] A. Seshadri, N.R. de Tacconi, C.R. Chenthamarakshan and K. Rajeshwar, *Electrochem. Solid-State Lett.* 9 (2006), p. C1

[21] D.K. Zhanga, Y.C. Liua,b,, Y.L. Liub, H. Y, *Physica B* 351 (2004) 178–183

[22] P. E. de Jongh, D. Vanmaekelbergh, and J. J. Kelly, *Chem. Mater.* 1999, *11*, 3512-3517

[23] Teresa D. Golden, Mark G. Shumsky, Yanchun Zhou, Rachel A. VanderWerf, Robert A. Van Leeuwen, and Jay A. Switzer, *Chem. Mater.* 1996, *8*, 2499-2504

[24] L.C. Wang, N.R. de Tacconi, C.R. Chenthamarakshan, K. Rajeshwar, M. Taoc, *Thin Solid Films* 515 (2007) 3090–3095

[25] T. Mahalingam, J.S.P. Chitra, S. Rajendran, M. Jayachandran, Mary Juliana Chockalingam, *Journal of Crystal Growth* 216 (2000) 304}310

[26] T. Mahalingama,b,*, J.S.P. Chitraa, G. Ravic, J.P. Chub, P.J. Sebastiand , *Surface and Coatings Technology* 168 (2003) 111–114

[27] S.S. Jeong, A. Mittiga, E. Salza, A. Masci, S. Passerini, *Electrochimica Acta* 53 (2008) 2226–2231

[28] Qing Wang; Kai Zhu; Nathan R. Neale; Arthur J. Frank, *Nano Lett.*, 2009, 9 (2), 806–813

[29] R. Kern, R. Sastrawan, J. Ferber, R. Stangl, J. Luther, *Electrochimica Acta* 47 (2002) 4213-4225

[30] Juan Bisquert, *J. Phys. Chem. B* 2002, 106, 325-333

[31] T. Hoshikawa, M. Yamada, R. Kikuchi, and K. Eguchi, *Journal of The Electrochemical Society*, 152 (2)E68-E73 (2005)

[32] Yanchun Zhou and Jay A. Switzer, *Scripta Materialia*, Vol. 38, No. 11, pp. 1731–1738, 1998

[33] Yueh-Hsun Lee, Ing-Chi Leu, Cheng-Lung Liao, Kuan-Zong Fung, *Journal of Alloys and Compounds* 436 (2007) 241-246

[34] D. K. Zhang; Y. C. Liu; Y. L. Liu; H. Yang, *Physica B* 2004, 351, 1-2, 178–183.

[35] Qing Wang; Kai Zhu; Nathan R. Neale; Arthur J. Frank , *Nano Lett.*, 2009, 9 (2), 806–813.

[36] Eric W. Bohannan, Ling-Yuang Huang, F. Scott Miller, Mark G. Shumsky, and Jay A. Switzer, *Langmuir* 1999,15,813-818

[37] S. Leopold, M. Herranen, and J.-Q. Carlsson, *Journal of The Electrochemical Society*, 148 (8) C513-C517 (2001)

[38] Yong Cai Zhang; Jing Yuan Tang; Gen Lin Wang; Ming Zhang; Xiao Ya Hu , *J. Crys. Growth* 2006, 294, 278–282.

[39] Wei-Tang Yao; Shu-Hong Yu; Yong Zhou; Jun Jiang; Qing-Song Wu; Lin Zhang; Jie Jiang, *J. Phys. Chem. B* 2005, 109, 14011–14016.

[40] S.Poulston, P.M. Parlett, P.Stone and M. Bowker, S*URFACE AND INTERFACE ANALYSIS*, VOL.24, 811-820 (1996)

[41] Peng Wang; Shaik M. Zakeeruddin; Pascal Comte; Raphael Charvet; RobinHumphry-Baker; Michael Grätzel, *J. Phys. Chem. B* 2003, 107, 14336–14341.

[42] Wei-Tang Yao; Shu-Hong Yu; Yong Zhou; Jun Jiang; Qing-Song Wu; Lin Zhang; Jie Jiang, *J. Phys. Chem. B* 2005, 109, 14011–14016.

[43] S.Poulston, P.M. Parlett, P.Stone and M. Bowker, S*URFACE AND INTERFACE ANALYSIS*, VOL.24, 811-820 (1996)

[44] M. Zistler, P. Wachter, C. Schreiner, M. Fleischmann, D. Gerhard, P. Wasserscheid, A. Hinsch, and H.J. Gores, *Journal of The Electrochemical Society*, 154 (9) B925-B930 (2007)

[45] R. van de Krol, A. Gossens, and J. Schoonman, *J. Electrochem. Soc.* Vol.144, No. 5, May 1997

[46] Francisco Fabregat-Santiago, Germa Garcia-Belmonte, Juan Bisquert, Peter Bogdanoff, and Arie Zaban, *Journal of The Electrochemical Society*, 150 (6) E293-E298 (2003)

[47] Anahita Mani, Carolien Huisman, Albert Goossens, and Joop Schoonman, *J. Phys. Chem. B* 2008, 112, 10086-10091

[48] W.B. Wu, Z.G. Jin, G.D. Hu, S.J. Bu, *Electrochemica Acta* 52(2007) 4804-4808

簡歷

姓名：許文朋

性別：男

出生：民國74年3月22日

籍貫：台灣省台北縣

學歷：國立中興大學電機工程學系

［ 92年9月 － 96年6月 ］

國立交通大學電子研究所碩士班

［ 96年9月 － 98年8月 ］

碩士論文題目：

對於電化學沉積的氧化亞銅/二氧化鈦塊材異質接面特性的研究

Characterization of Electrochemically Deposited Cu_2O/TiO_2 Bulk Hetero-Junction